

Effective permeability of fluvial lithofacies in the Bunter Sandstone Formation, UK

Hossain, Shakhawat; Hampson, Gary J.; Jacquemyn, Carl; Jackson, Matthew D.; Petrovskyy, Dmytro; Geiger, Sebastian; Silva, Julio D.Machado; Judice, Sicilia; Rahman, Fazilatur; Sousa, M. Costa

DOI

[10.1016/j.advwatres.2025.104936](https://doi.org/10.1016/j.advwatres.2025.104936)

Publication date

2025

Document Version

Final published version

Published in

Advances in Water Resources

Citation (APA)

Hossain, S., Hampson, G. J., Jacquemyn, C., Jackson, M. D., Petrovskyy, D., Geiger, S., Silva, J. D. M., Judice, S., Rahman, F., & Sousa, M. C. (2025). Effective permeability of fluvial lithofacies in the Bunter Sandstone Formation, UK. *Advances in Water Resources*, 199, Article 104936. <https://doi.org/10.1016/j.advwatres.2025.104936>

Important note

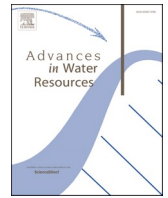
To cite this publication, please use the final published version (if applicable). Please check the document version above.

Copyright

Other than for strictly personal use, it is not permitted to download, forward or distribute the text or part of it, without the consent of the author(s) and/or copyright holder(s), unless the work is under an open content license such as Creative Commons.

Takedown policy

Please contact us and provide details if you believe this document breaches copyrights. We will remove access to the work immediately and investigate your claim.



Effective permeability of fluvial lithofacies in the Bunter Sandstone Formation, UK

Shakhawat Hossain^{a,b,*}, Gary J. Hampson^a, Carl Jacquemyn^a, Matthew D. Jackson^a, Dmytro Petrovskyy^{a,c}, Sebastian Geiger^c, Julio D. Machado Silva^d, Sicilia Judice^d, Fazilatur Rahman^d, M. Costa Sousa^d

^a Department of Earth Science and Engineering, Imperial College London, London, SW7 2AZ, UK

^b Department of Geology, University of Dhaka, Dhaka 1000, Bangladesh

^c Department of Geoscience and Engineering, Delft University of Technology, 2600 AA Delft, The Netherlands

^d Department of Computer Science, University of Calgary, Canada

ARTICLE INFO

Keywords:

Bunter Sandstone Formation
Effective permeability
Fluvial
Lithofacies modelling
Kv/Kh

ABSTRACT

Understanding effective permeability is crucial for predicting fluid migration and trapping in subsurface reservoirs. The Bunter Sandstone of northwestern Europe hosts major groundwater and geothermal resources and is targeted for CO₂ storage projects. Here the effective permeability of fluvial facies within the Bunter Sandstone Formation was assessed using facies-scale models. Twelve lithofacies were modeled based on core and outcrop observations of their geometries and dimensions. Permeability values from minipermeameter measurements were assigned to low- and high-permeability lithologies in each facies. The dimensions of a Representative Elementary Volume (REV) in depositional dip, depositional strike and vertical directions were determined by extracting sub-volumes from the models at different scales, calculating values of effective permeability for each sub-volume, and identifying the sub-volume at which the values of effective permeability stabilise as the REV. The REV dimensions vary with facies type and flow direction, but are typically of order tens of centimetres to metres in size, significantly larger than a typical core plug. Having identified the REV, we analyze the effective permeabilities of the different facies types. Normalized values of effective permeabilities in depositional dip, strike and vertical directions (k_d , k_s , k_v), relative to the permeability of low- and high-permeability lithologies in each facies, display a positive linear correlation with the proportion of high-permeability lithology (clay-poor sandstone) for all facies. Therefore, the proportion of clay-poor sandstone, as measured in core data, can be used to predict facies-scale effective permeability in the Bunter Sandstone Formation, as well as in analogous fluvial deposits globally.

1. Introduction

Triassic fluvial sandstones in northwestern Europe form important groundwater aquifers (Allen et al., 1997; Heinemann et al., 2012; Noy et al., 2012; Medici and West, 2022) and geothermal reservoirs (Downing et al., 1984; Gérard et al., 2006; Yousaf et al., 2023), and are being actively evaluated and developed for CO₂ storage (Gluyas and Bagudu, 2020; Bossennec et al., 2021; Hartemink, 2021; Bertier et al., 2022; Alshakri et al., 2023; Bofill et al., 2024; Cecchetti et al., 2024; Hossain et al., 2024) and Aquifer Thermal Energy Storage (ATES) (Adams et al., 1980; Holmslykke et al., 2021; Jackson et al., 2024), essential for achieving net-zero emission targets and sustainable growth.

Accurate reservoir characterisation, including estimating effective permeability of different facies and modeling their spatial distribution, is paramount for successful project development in aquifer management, geothermal applications, and CO₂ storage.

In a typical reservoir modelling workflow, values of permeability used to populate geological models are derived from core plug data and estimated from wireline logs through empirical equations (Helle et al., 2001; Mania, 2017). The volumes of model grid cells are several orders of magnitude larger than those of core plugs (Corbett and Jensen, 1992). Permeability values are typically categorized by facies type and then averaged at the grid-block level, a process known as 'blocking' (Jackson et al., 2003). However, this process may not accurately represent the

* Corresponding author at: Department of Earth Science and Engineering, Imperial College London, London, SW7 2AZ, UK.

E-mail address: shakhawat.geo@du.ac.bd (S. Hossain).

<https://doi.org/10.1016/j.advwatres.2025.104936>

Received 15 December 2024; Received in revised form 17 February 2025; Accepted 24 February 2025

Available online 25 February 2025

0309-1708/© 2025 The Author(s). Published by Elsevier Ltd. This is an open access article under the CC BY license (<http://creativecommons.org/licenses/by/4.0/>).

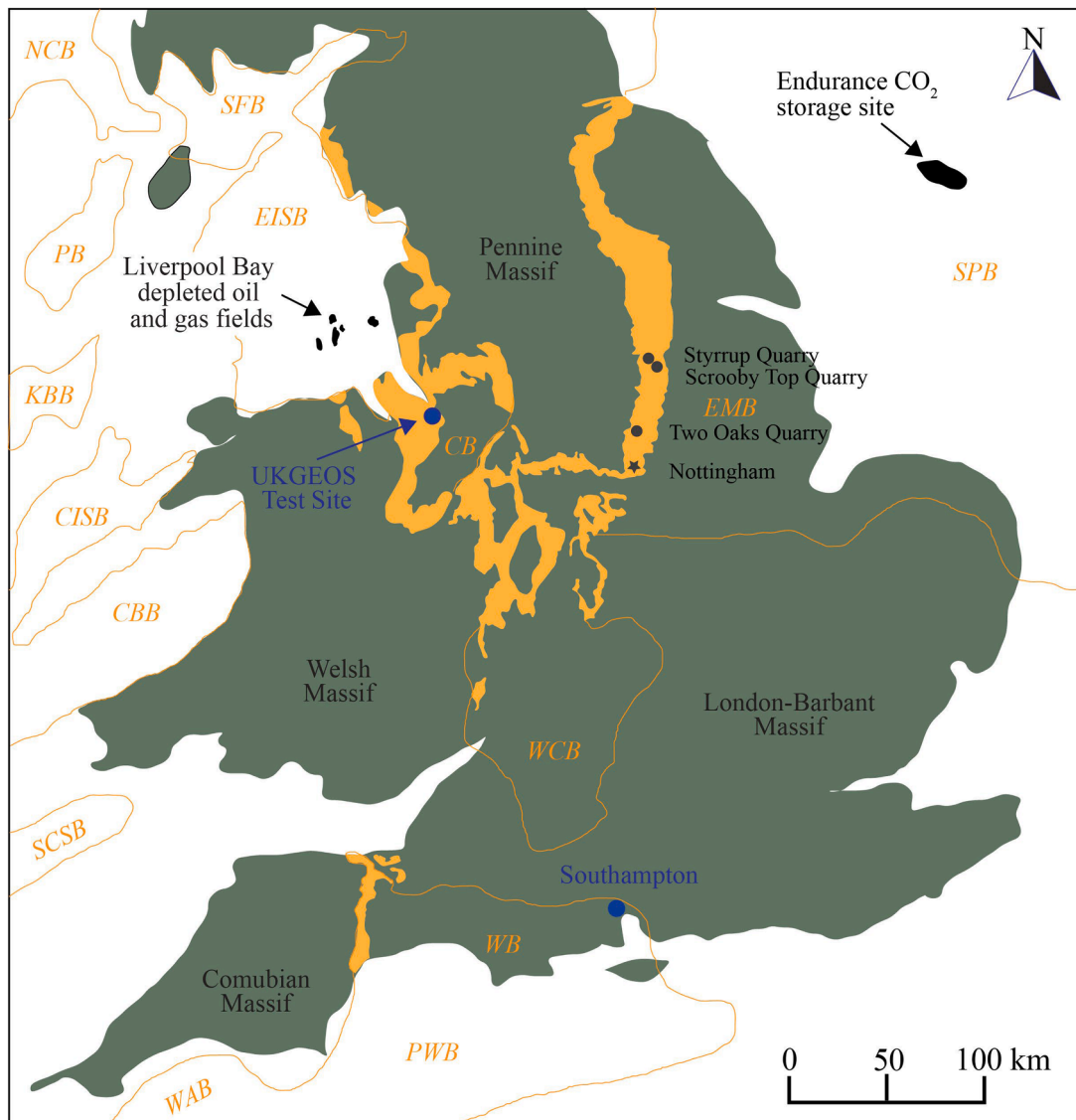


Fig. 1. Map showing the distribution of Sherwood Sandstone Group (SSG) outcrops (in orange) across the onshore UK and their presence in subsurface reservoirs (modified after [English et al., 2024](#)). The approximate boundaries of the preserved SSG are outlined with orange lines. Grey circles mark the locations of the Styrrup, Two Oaks, and Scrooby Top quarries, while Nottingham outcrops are indicated by a star. Sedimentary basins that contain the Sherwood Sandstone Group are: CB, Carlisle Basin; CBB, Cardigan Bay Basin; CISB, Central Irish Sea Basin; EISB, East Irish Sea Basin; EMB, East Midlands Basin; KBB, Kish Bank Basin; LB, Larne Basin; NCB, North Channel Basin; NCSB, North Celtic Sea Basin; PB, Peel Basin; PWB, Portland Wight Basin; SCSB, South Celtic Sea Basin; SFB, Solway Firth Basin; SPB, Southern Permian Basin; WB, Wessex Basin; WAB, Western Approaches Basin; WCB, Worcester Basin.

underlying permeability structure unless the latter has a specific spatial distribution, such as simple parallel layering. Previous studies indicate that averaging core-plug permeability measurements is inadequate for grid-block scale analysis, because it fails to represent geological heterogeneity ([Jackson et al., 2003, 2005](#); [Nordahl and Ringrose, 2008](#); [Nordahl et al., 2014](#)). To ensure accuracy at larger scales, a Representative Elementary Volume (REV) of the rock, which defines the smallest volume over which measurements can reliably represent the entire rock body, must be utilized ([Bear, 1972](#)). This ensures consistency in properties regardless of the sample volume considered. The REV for permeability needs to be large enough to encompass flow variations in all directions. However, it can be challenging to define the REV in practice due to the overlapping nature of spatial scales of heterogeneity ([Nordahl and Ringrose, 2008](#)).

Several techniques have been employed to determine effective permeability through REV analysis. [Jackson et al. \(2003, 2005\)](#) used serial sectioning of large rock specimens (measuring several tens of centimetres in each direction) to reconstruct sandbody geometry and

connectivity in 3D models, and thereby characterize the reservoir properties of heterolithic tidal sandstone facies. [Massart et al. \(2016\)](#) used a surface-based modeling technique to investigate the impact of mudstone drape distribution on the effective permeability of heterolithic, cross-bedded tidal sandstones with 3D models. [Nordahl et al. \(2014\)](#) and [Lottman \(2019\)](#) utilized process-oriented modeling techniques to estimate the REV of heterolithic tidal sandstones and meandering fluvial deposits, respectively. In this study, we employ a novel sketch-based modeling technique ([Jacquemyn et al., 2021](#)) to create models of sedimentological facies. The novelty of this study lies in the fact that, for the first time, we have created deterministic lithofacies scale models by sketching lithological heterogeneity directly from outcrop photos and then used computationally efficient, single-phase flow diagnostics that are integrated into the sketch-based modelling tool ([Petrovskyy et al., 2023](#)) to determine the REV for the different facies.

This study focusses on characterizing the Bunter Sandstone Formation, which comprises fluvial and aeolian deposits. The main objective is

Table 1

Fluvial facies in the studied Bunter Sandstone Formation cores and Sherwood Sandstone Group outcrops (after Hossain et al., 2024). Permeability data are from well 42/25d-3, Endurance CO₂ storage site, southern North Sea (Fig. 1).

Lithofacies	Description	Minipermeability (mD)	Core plug Permeability (mD)
Planar cross-bedded sandstone (Sp)	Fine- to medium-grained, moderately sorted sandstone arranged in sets of planar cross beds. Individual cross-sets are 40–120 cm thick. Both topsets and bottomsets are horizontal to slightly inclined. Foresets consist of alternating clay-poor and clay-rich sandstone laminae.	6–8600	9.5 –5350
Trough cross-bedded sandstone (St)	Medium- to fine-grained, trough cross-bedded sandstone. Individual sets are 40–80 cm thick.	90–7800	13 – 2813
Planar cross-bedded sandstone with mud clasts along foresets (Spmc)	Well-sorted, fine- to medium-grained, planar cross-bedded sandstone with mud clasts along foresets. Clasts are rounded and 2–4 cm in diameter.	2 –3900	4–3853
Parallel-laminated sandstone (Sh)	Fine-grained, well-sorted sandstone containing planar-parallel lamination. Clay-rich laminae are present. Thickness ranges from 50 to 150 cm.	24–900	7.2–2468
Mottled and deformed sandstone (Smd)	Fine-grained sandstone with deformation in the form of harmonic and disharmonic folds, antiformal shapes, and subvertical pipes.	0.2–1600	2.8–480
Matrix-supported conglomerate (Gmg)	Fine- to coarse-grained sandstone matrix with grey, pebble-sized (1–4 cm diameter) mudstone clasts. Clasts are sub-rounded to sub-angular.	0.06–80	0.7–89
Fine-grained sandstone and siltstone (Sss)	Siltstone with subordinate thin (20–50 cm) beds of fine-grained sandstone. Sandstones are typically cross-bedded. Units contain abundant sand-filled desiccation cracks.	10–70	1.14–588
Low angle cross-bedded sandstone (Sl)	Fine- to medium-grained, moderately sorted, low-angle cross-bedded sandstone. Individual set thickness is 20–30 cm.	170–700	35–1673
Laminated mudstone (Fl)	Laminated, dark brown mudstone with rare siltstone laminae. Units are typically 10–20 cm thick, and rarely up to 50 cm thick.	0.08–3	0.18–2.92

Table 1 (continued)

Lithofacies	Description	Minipermeability (mD)	Core plug Permeability (mD)
Structureless sandstone (Sm)	Fine- to medium-grained, moderately to well sorted sandstone with erosional base. Units are 30–50 cm thick and often overlie mudstone units.	20–1300	9.5 –5350
Trough cross-laminated sandstone (St1)	Multiple sets of fine- to medium-grained, moderately sorted, trough cross-laminated sandstone. Individual sets are 10–15 cm thick, and cosets are 60–100 cm thick. Dark colored, clay-rich laminae are present along the troughs.	80–190	35–1673
Crinkly laminated sandstone (Sc)	Thin units (10–20 cm) of siltstones and very fine-grained sandstones with irregular to highly diffuse, crinkly and variably continuous lamination.	0.4–240	0.69–180

to assess the impact of sedimentological heterogeneity on the effective permeability of the fluvial sedimentological facies within the Bunter Sandstone Formation. To achieve this, we build on previous work that has identified and interpreted the sedimentological facies from cores and outcrops, and characterized the permeability of these facies at the lamina scale using minipermeametry and core plug analysis (Hossain et al., 2024). In this paper, we document: (1) the construction of facies-scale reservoir models of all lithofacies at resolutions capable of capturing the heterogeneity associated with each facies; (2) population of these models with appropriate lamina- and bed-scale permeability values; and (3) analysis of the models to determine the REV for each lithofacies, and thus determine their effective permeability in depositional dip, depositional strike and vertical directions.

2. Geological context and resources

The Sherwood Sandstone Group of the onshore UK, and the correlative Bunter Sandstone Formation of the offshore UK, represents a succession of continental ‘red beds’ deposited in several rift basins in the Triassic period (Ambrose et al., 2014). The dominant lithologies of this unit are sandstones and pebbly sandstones with varying amounts of conglomerates, siltstones and claystones (e.g. Ambrose et al., 2014; Medici et al., 2015; Wakefield et al., 2015). The unit is found in the Wessex, Worcester, Cheshire, East Irish Sea, Solway and Carlisle basins (Fig. 1). Its thickness varies considerably, from as little as 90 m in south Nottinghamshire to over 600 m in Lancashire (Hounslow and Ruffell, 2006; McKie and Williams, 2009; Ambrose et al., 2014). The Sherwood Sandstone Group is interpreted to constitute fluvial-aeolian deposits (e.g. Medici et al., 2019).

The lower part of the Sherwood Sandstone is fluvial, and passes from fluvial conglomerates and pebbly sandstones in the basins of western England to medium- to fine-grained sandstones in the basins of north-eastern England (Holliday et al., 2008; Ambrose et al., 2014). The upper part of the Sherwood Sandstone contains aeolian facies, particularly in northwestern England (Holliday et al., 2008; Medici et al., 2019). The upward change in depositional setting has been attributed to the avulsion of river channels or the onset of aeolian sediment supply (Holliday et al., 2008; Ambrose et al., 2014). High subsidence rates allowed the

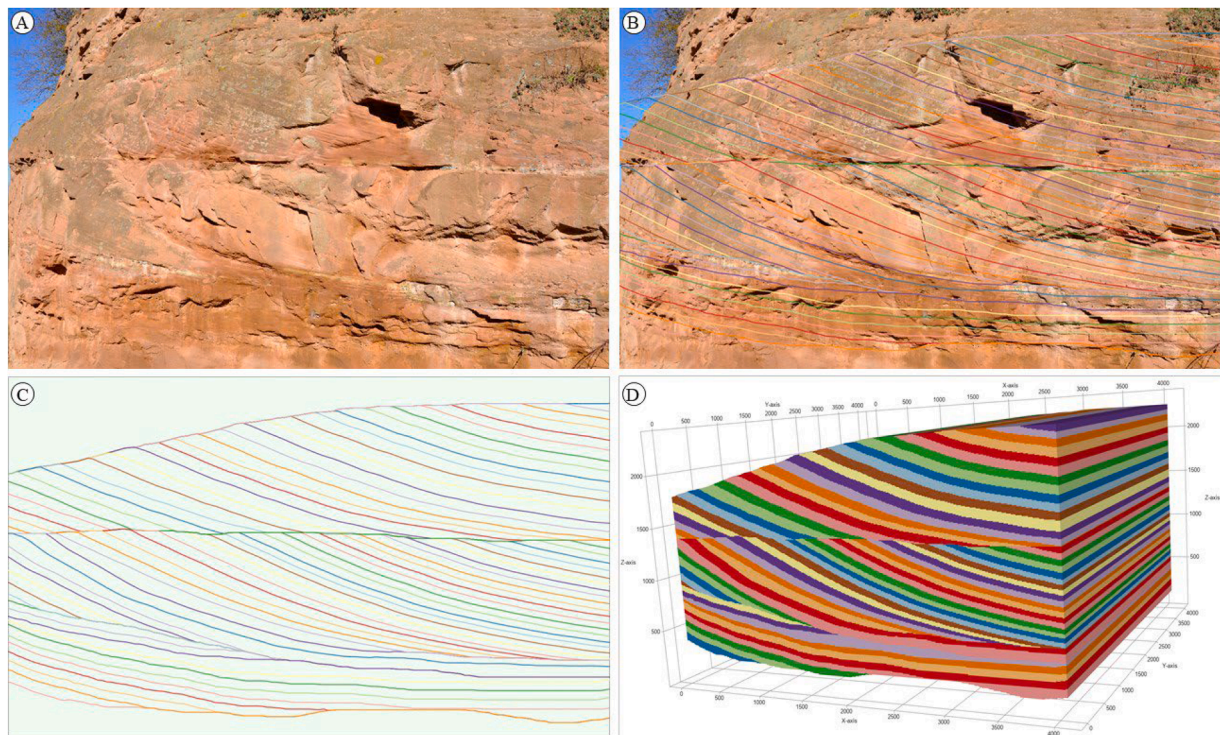


Fig. 2. Construction of a sketch-based 3D model, using the example of planar cross-bedded sandstone (Sp) facies (Table 1). A) Outcrop photo of planar cross-bedded sandstone (Sp) facies at Styrrup Quarry (Fig. 1); B) lines sketched over cross-set bounding surfaces and foresets in photo, and C) with photo removed; and D) 3D model with sketched surfaces extrapolated perpendicular to the plane of the photo.

preservation of aeolian facies in western England, whereas the absence of these facies in eastern England is postulated to reflect low subsidence rates (Meckel et al., 2015; Medici et al., 2019).

Sandstones in the Sherwood Sandstone Group exhibit significant variability in petrophysical properties across different basins. Porosity ranges from 3 to 38 %, while hydraulic conductivity spans from 0.1 to 11,000 mD (Cowan, 1993; Allen et al., 1997; Brookfield, 2004; Pokar et al., 2006). In the Cheshire Basin, permeability varies from 1 to 7900 mD (Bloomfield et al., 2006). In the Hewett gas field of the southern North Sea, average permeabilities of 500 mD and 1000 mD have been reported for the upper and lower Bunter Sandstone Formation (Cooke-Yarborough, 1991). Within the Sherwood Sandstone Group of the Irish Sea, permeability of fluvial facies ranges from 0.1 to 1000 mD, whereas that of aeolian facies ranges from 1 to 3000 mD (Meadows and Beach, 1993). Aeolian facies typically exhibit higher permeability than fluvial facies due to their lower clay content (Wakefield et al., 2015; Medici et al., 2019). Low-permeability zones are often associated with mudstones deposited in overbank and lacustrine environments.

The Sherwood Sandstone Group and Bunter Sandstone Formation hold significant economic importance due to their lithological characteristics and stratigraphic position below thick sealing mudstones and evaporites of the Mercia Mudstone Group and Dowsing Formation (e.g. Wakefield et al., 2015; Medici et al., 2019). These sandstones host groundwater resources in the Midlands and Cheshire basins of the onshore UK, and are targets for carbon dioxide (CO₂) storage projects both onshore and offshore UK (Gluyas and Bagudu, 2020; Hollinsworth et al., 2024; Hossain et al., 2024). Moreover, the Sherwood Sandstone Group is a source of low-enthalpy geothermal energy, as demonstrated by the Southampton Geothermal District Heating Scheme (Downing et al., 1984). The Sherwood Sandstone Group is a focus of the UK Geoenery Observatories (UKGEOS) initiative in the Cheshire Basin (Kingdon et al., 2019), which aims to advance research in subsurface energy technologies such as geothermal energy extraction and carbon capture and storage (CCS).

Across northwestern Europe, the equivalents of the Sherwood Sandstone Group and Bunter Sandstone Formation play critical roles in sustainable resource projects. In The Netherlands, the Lower and Main Buntsandstein subgroups serve as aquifers (Cecchetti et al., 2024), and the Trias Westland Geothermal Project explores the geothermal potential of these formations to provide sustainable heating (Yousaf et al., 2023). The Porthos Project in the Port of Rotterdam investigates the use of these formations for CO₂ storage beneath the Southern North Sea (Sorbier, 2024). In Germany, the Buntsandstein Group hosts groundwater aquifers and is being investigated for geothermal energy applications (Vandeweyer et al., 2009). The Ketzin Pilot Site, Europe's longest-running onshore CO₂ storage project, also uses the Buntsandstein Group as its storage unit (Martens et al., 2013). In France, the Buntsandstein Group hosts aquifers in the Alsace region (Bofill et al., 2024).

3. Dataset and methods

3.1. Core and outcrop facies analysis

Core data from wells 42/25-1 and 42/25d-3, spanning intervals of 10 m and 163 m respectively, from the Endurance CO₂ storage site, offshore UK, were analyzed to develop a lithofacies scheme highlighting small-scale sedimentological heterogeneity (Hossain et al., 2024).

The studied cores provide a detailed and continuous record of facies in vertical succession, but do not constrain their lateral extent. Thus, outcrop analogues are crucial for understanding the dimensions, geometry and lateral extent of the facies. We collected such data from exposures of the Sherwood Sandstone Group, from several quarries (e.g., Styrrup Quarry, Scrooby Top Quarry, Two Oaks Quarry) and other mined faces (e.g., Park Tunnel, Nottingham Castle) in the East Midlands, onshore UK (Fig. 1; see also similar data collected by Medici et al., 2015, 2019; Wakefield et al., 2015). The resulting lithofacies scheme is described in detail in Hossain et al. (2024) and summarized in Table 1.

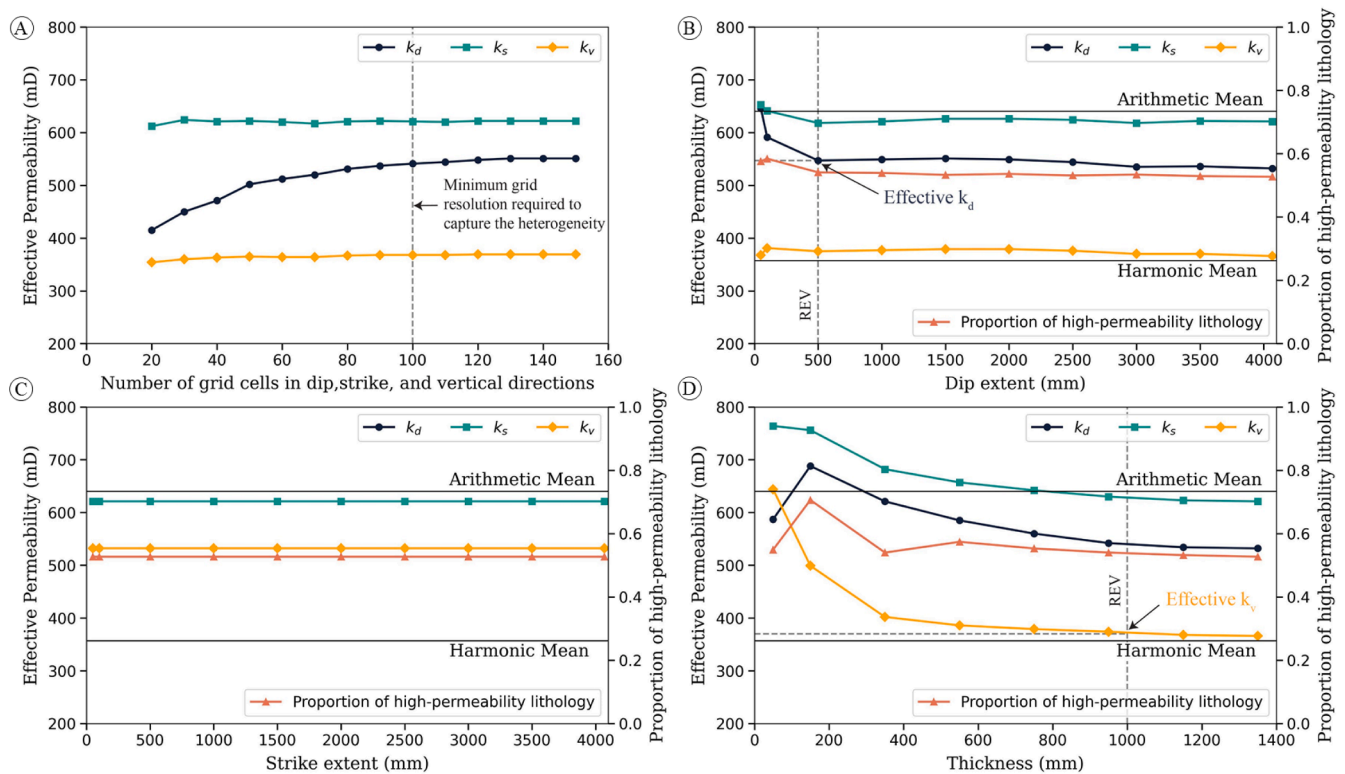


Fig. 3. Plots illustrating how appropriate model resolution and REV dimensions are determined, exemplified by the model of planar cross-bedded sandstone (Sp) facies (Fig. 2). A) Effective permeability in the depositional dip (k_d), depositional strike (k_s) and vertical (k_v) directions plotted against the number of grid cells in the dip, strike and vertical directions, to establish the minimum grid resolution that captures characteristic heterogeneity. Vertical dashed line shows the minimum resolution required to capture the heterogeneity related to these facies. B-D) Effective permeability (k_d , k_s , k_v) plotted against increasing model dimensions: B) along depositional dip, C) along depositional strike, and D) vertically, to establish REV dimensions. Values of arithmetic and harmonic means, and the proportion of high-permeability lithology (clay-poor sandstone in this facies) in each model sub-volume are shown for comparison. Vertical and horizontal dashed lines show the REV dimension and the effective permeability, respectively, along the depositional dip and vertical directions.

3.2. Minipermeameter data

Permeability data were collected from selected intervals of the core from well 42/25d-3 using a portable hand-held air permeameter on a grid, to capture the effects of lamina-scale heterogeneity in each facies (Hossain et al., 2024). These permeability data are documented in (Hossain et al. 2024) and summarized for each facies in Table 1.

3.3. Construction of facies-scale reservoir models

Deterministic models of the lithofacies (Table 1) were constructed using sketch-based reservoir modelling techniques implemented in open-source research code (Rapid Reservoir Modelling, RRM; (Costa Sousa et al., 2020; Jacquemyn et al., 2021; Petrovskyy et al., 2023). An example of this approach is shown in Fig. 2. The dimensions and geometrical configuration of lithologies in the facies were identified in the cores and outcrops (Hossain et al., 2024). Bedding-perpendicular cross-sections derived from photos of outcrop faces and cores are combined with bedding-plane maps derived from outcrops and/or conceptual 3D block diagrams in constructing stratal surfaces and the volumes that the surfaces bound in the sketch-based models (Jacquemyn et al., 2021). Our approach uses sketch-based interface and modelling computational methods to preserve the geometry of geological features critical to reservoir characterization in the resulting models.

In the planar cross-bedded sandstone (Sp), low-angle cross-bedded sandstone (Sl), and parallel-laminated sandstone (Sh) facies, stratal surfaces identified in the depositional dip direction are continuous and parallel in the depositional strike direction. For these facies, stratal surfaces sketched as lines in depositional-dip-oriented cross-sections

were simply extrapolated horizontally along depositional strike. For facies such as trough cross-bedded sandstone (St), trough cross-laminated sandstone (Stl), and crinkly laminated sandstone (Sc), stratal surfaces sketched as lines in depositional-dip-oriented cross-sections were extruded along sketched map-view trajectories to depict accurately the 3D stratal architecture (cf. Fig. 6 in Costa Sousa et al., 2020). Stratal surfaces in facies with more complex 3D architecture, such as mottled and deformed sandstone (Smd) facies, were generated by interpolating sketched lines between successive map-view planes (cf. Fig. 6A–C in Jacquemyn et al., 2021).

For two facies, planar cross-bedded sandstone with mud clasts along foresets (Spmc) and matrix-supported conglomerate (Gmg), sketch-based models were supplemented by sequential indicator simulation (SIS) and object-based modelling techniques to distribute pebbles as objects along foresets. The resulting pebble distribution in the models was visually inspected and compared with outcrop photographs as a check of model quality.

3.4. Model resolution

Determining the lowest model resolution that captures the continuity and connectivity of laminae and beds of contrasting permeability is necessary before calculating effective properties in the models. Below, the process of identifying the required model resolution is demonstrated for planar cross-bedded sandstone (Sp) facies as an example (Fig. 3). After constructing the model, its resolution was varied and the corresponding effective permeability was calculated in depositional dip (k_d), depositional strike (k_s), and vertical (k_v) directions using single-phase flow diagnostics implemented in RRM (Petrovskyy et al., 2023). Flow

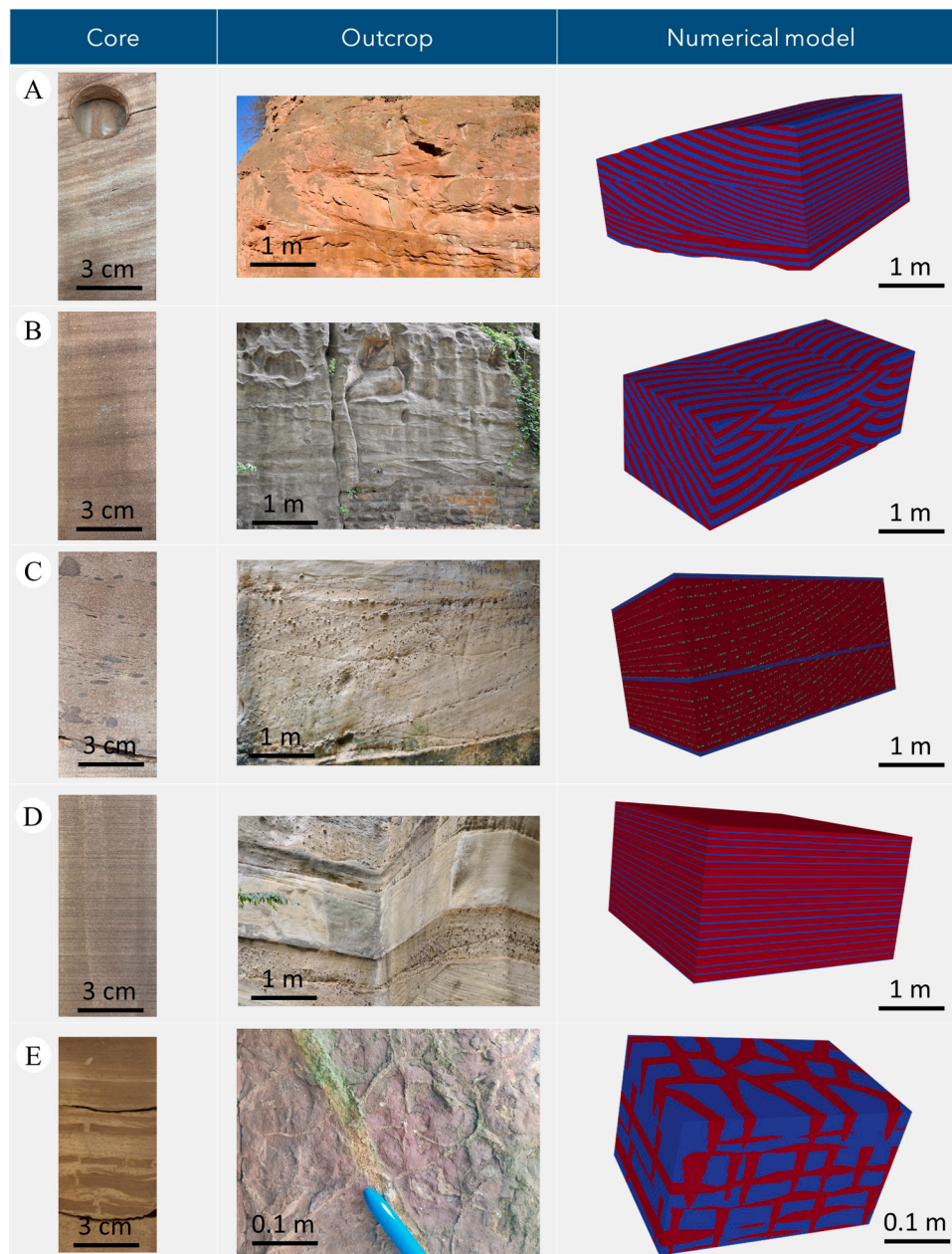


Fig. 4. Core photos, outcrop photos, and perspective views of 3D reservoir models showing the geometrical configuration of relatively high (red) and relatively low (blue) permeability lithologies in each facies (Table 1). A) trough cross-bedded sandstone (St), B) planar cross-bedded sandstone (Sp), C) planar cross-bedded sandstone with mud clasts along foresets (Spmc), D) parallel-laminated sandstone (Sh), E) mottled and deformed sandstone (Smd), F) matrix-supported conglomerate (Gmg), G) fine-grained sandstone and siltstone (Sss), H) low-angle cross-bedded sandstone (Sl), I) laminated mudstone (Fl), J) structureless sandstone (Sm), K) trough cross-laminated sandstone (Stl), and L) crinkly laminated sandstone (Sc). Core and outcrop photos are taken from well 42/25d-3 and various outcrops of the Bunter Sandstone Formation in the East Midlands (Fig. 1), respectively, except for outcrop photos in Fig. 4K (Hossain et al., 2023) and Fig. 4L (Sansom, 1992).

diagnostics rely on a reduced-physics, single-phase pressure solution to calculate key flow properties in a rapid, computationally efficient manner (Shahvali et al., 2012; Rasmussen and Lie, 2014; Lie et al., 2015; Møyner et al., 2015). An orthogonal grid is used for flow diagnostic calculations, to ensure numerical stability (Petrovskyy et al., 2023). Permeability is calculated in each of the three orthogonal directions in the model by imposing a uniform pressure over opposing inlet and outlet faces, setting all other faces to have zero flow, and simulating the resulting single phase flow assuming unit fluid viscosity. The effective permeability is then simply given by the total flow rate divided by the pressure gradient (Petrovskyy et al., 2023).

To test the sensitivity of effective k_d , k_s , and k_v to grid resolution, the

number of grid cells in each direction was plotted against the values of k_d , k_s , and k_v for each model resolution (Fig. 3A). The number of grid cells was increased (thus increasing grid resolution) until values of k_d , k_s , and k_v converged to a stable value. Fig. 3A shows the fluctuating nature of effective permeability values until they reach a stable value at the minimum grid resolution required to capture the heterogeneity that is characteristic of a particular facies. Depending on their internal geometrical complexity, different facies require different model resolutions. Resolution was determined before undertaking the REV analysis for a given facies.

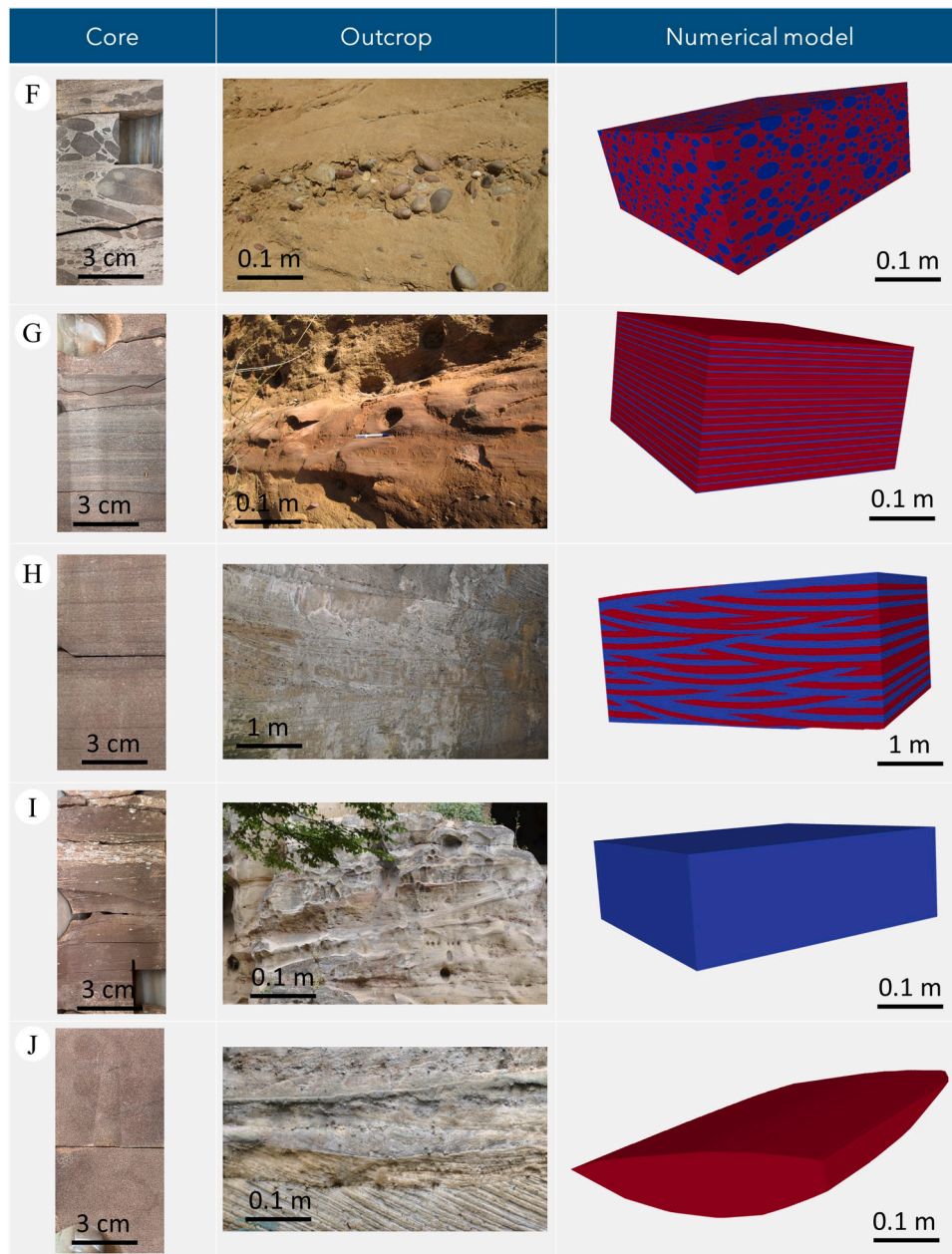


Fig. 4. (continued).

3.5. Identification of representative elementary volume (REV)

After determining the model resolution, the next step is to identify the REV, and thereby to obtain representative values of k_d , k_s and k_v . Most facies contain two lithologies, which are assigned a single value of permeability, corresponding to the arithmetic mean of mini-permeameter measurements for that lithology in the facies in the core from well 42/25d-3 (Hossain et al., 2024). These facies therefore contain a low-permeability and a high-permeability lithology. The initial sketch-based model of a particular facies is large relative to the heterogeneities that are characteristic of that facies (e.g., foreset-lamina extent in a planar cross-bed set; Fig. 2D). To find the REV dimensions in the depositional dip, depositional strike, and vertical directions, the sides of the initial model that are perpendicular to the direction of interest were progressively cropped, to generate a sub-volume of the model, and the effective permeability in all three directions was calculated for the model sub-volume. Effective permeability was then plotted

against the model dimension in the direction of interest. At small volumes, effective permeability shows oscillations due to non-representative sampling of heterogeneities. At progressively larger volumes, the oscillations in effective permeability decrease in amplitude, and measurements of effective permeability stabilize. The model sub-volume at which values of effective permeability stabilize is identified as the REV, which is sufficiently large to characterise the heterogeneity of the facies (Jackson et al., 2003, 2005; Nordahl and Ringrose, 2008; Nordahl et al., 2014; Lottman, 2019). In the example of planar cross-bedded sandstone with continuous clay-rich foresets (Sp1) facies shown in Fig. 3B–D, the REV dimensions in depositional dip and vertical directions are 0.5 m and 1.0 m, respectively. Since beds and laminae maintain a uniform geometrical configuration in the depositional strike direction, there is no REV in that direction. The effective permeability along the dip and vertical directions is 547 mD and 370 mD, respectively. The arithmetic and harmonic means of permeability, weighted by the proportions of lithologies in the measured sub-volume of the model,

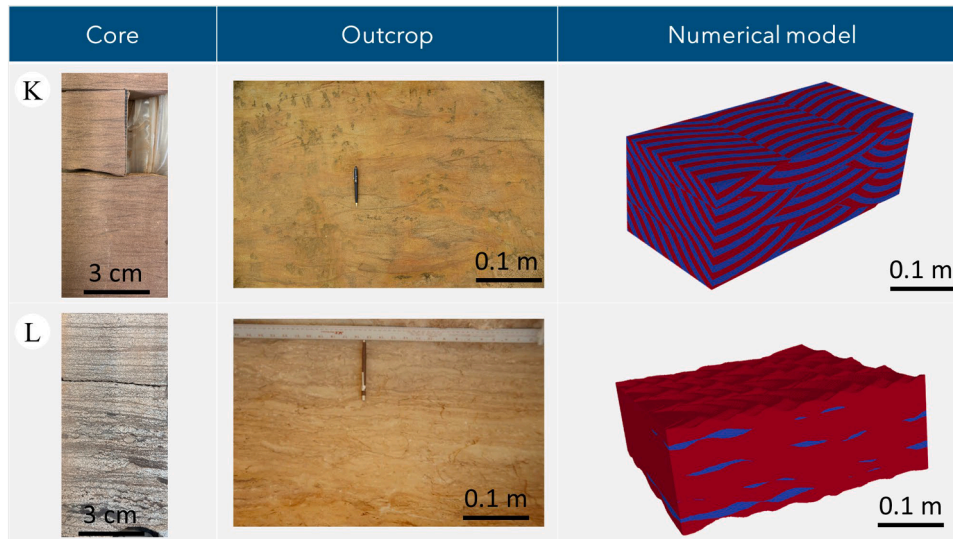


Fig. 4. (continued).

Table 2
Model resolution and element size required for different facies (n/a = not appropriate).

Facies	Number of grid cells (Dip × Strike × Vertical)	REV Dimensions (m) (Dip × Strike × Vertical)	Element Size (mm) (Dip × Strike × Vertical)
Planar cross-bedded sandstone with continuous clay-rich foresets (Sp1)	100 × 100 × 100	0.5 × n/a × 1	5 × 1 × 10
Planar cross-bedded sandstone with discontinuous clay-rich foresets (Sp2)	100 × 100 × 100	3.5 × n/a × 0.8	35 × 1 × 8
Trough cross-bedded sandstone with continuous clay-rich foresets (St1)	120 × 120 × 120	1.5 × 2 × 1.2	12.5 × 16.6 × 10
Trough cross-bedded sandstone with discontinuous clay-rich foresets (St2)	120 × 120 × 120	1 × 3 × 1.5	8.3 × 25 × 12.5
Planar cross-bedded sandstone with mud clasts along foresets (Spmc)	100 × 100 × 100	2.8 × n/a × 0.7	28 × 1 × 7
Parallel-laminated sandstone (Sh)	100 × 100 × 100	Layered	Layered
Mottled and deformed sandstone (Smd)	120 × 120 × 120	0.85 × 0.4 × 0.35	7 × 3.3 × 2.9
Matrix-supported conglomerate (Gmg)	100 × 100 × 100	0.3 × 0.3 × 0.4	3 × 3 × 4
Fine-grained sandstone and siltstone (Sss)	100 × 100 × 100	Layered	Layered
Low-angle cross-bedded sandstone (Sl)	80 × 80 × 80	2.3 × n/a × 1.3	30 × 1 × 15
Laminated mudstone (Fl)	Homogenous	Homogenous	Homogenous
Structureless sandstone (Sm)	Homogenous	Homogenous	Homogenous
Trough cross-laminated sandstone (St1)	120 × 120 × 120	0.2 × 0.5 × 0.1	1.6 × 4 × 0.8
Crinkly laminated sandstone (Sc)	60 × 60 × 60	0.3 × 0.6 × 0.15	5 × 10 × 3

were plotted for comparison with calculated values of effective permeability and to determine if these mean values can serve as proxies for k_d , k_s and k_v .

For each facies, normalized effective permeability (k_n) values in the depositional dip, depositional strike and vertical directions were determined using Eq. (1) (Jackson et al., 2005).

$$k_n = \frac{k_{eff} - k_{min}}{k_{max} - k_{min}} \quad (1)$$

Where, k_{eff} represents the effective permeability in a given direction at the representative elementary volume (REV), while k_{max} and k_{min} are the respective maximum and minimum permeability values used to populate the facies models (i.e., the values assigned to the low-permeability and high-permeability lithologies in the facies).

4. Results

4.1. Representation of lithofacies in sketch-based models

Trough cross-bedded sandstone (St) and trough cross-laminated sandstone (Stl) facies contain cross-sets of foreset laminae that are inclined down depositional dip and have a trough-shaped geometry along depositional strike (Fig. 4B, K). Mottled and deformed sandstone (Smd) and crinkly laminated sandstone (Sc) facies contain lenticular beds of sandstone and mudstone that are encased in a background of, respectively, mudstone and sandstone (Fig. 4E, L). Mottled and deformed sandstone (Smd) facies also contain downward-tapering, vertical sheets that are arranged in plan-view polygonal networks, representing desiccation crack fills, that span the mudstone layers and connect sandstone lenses. Matrix-supported conglomerate (Gmg) facies have a disorganised distribution of mud clasts in both depositional dip, depositional strike and vertical directions (Fig. 4F). Mud clasts vary in size from 10 to 40 cm and have a common azimuth, which corresponds to the palaeo-flow direction. Planar cross-bedded sandstone (Sp), planar cross-bedded sandstone with mud clasts along foresets (Spmc) and low-angle cross-bedded sandstone (Sl) facies have foreset laminae that are inclined down depositional dip and are horizontal along depositional strike (Figs. 4A, C, H). In planar cross-bedded sandstone with mud clasts along foresets (Spmc), impermeable mud clasts along the foresets form a discontinuous barrier. Parallel laminated sandstone (Sh) and fine-grained sandstone and siltstone (Sss) facies are horizontally layered in depositional dip and strike directions (Fig. 4D, G). Structureless mudstone (Sm) and laminated mudstone (Fl) facies form lenticular bodies with no internal lithological variation (Fig. 4I, J).

Minipermeameter data show that permeability variations of up to a factor of 5 occur within some facies, reflecting the lithological, grain size

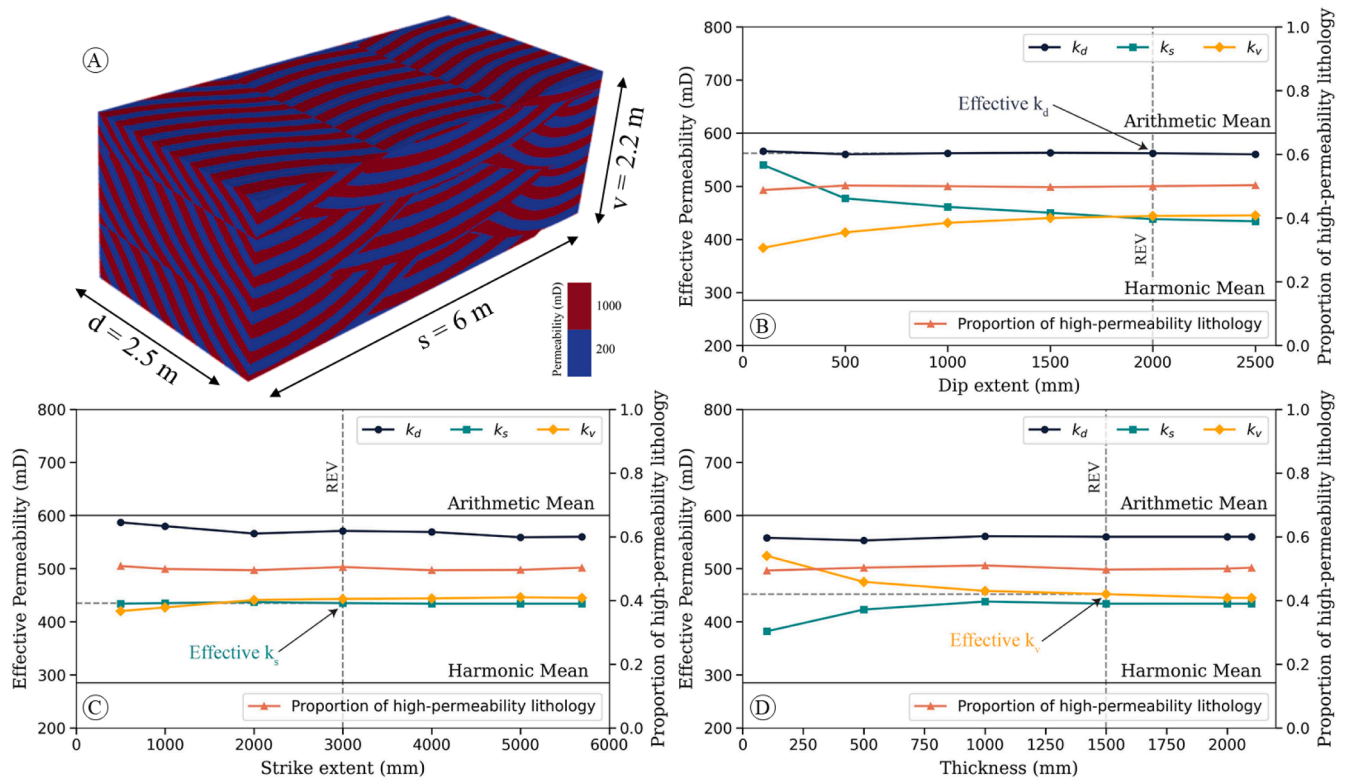


Fig. 5. A) Perspective view of the 3D model of the trough cross-bedded sandstone facies (St1; Table 1, Fig. 4B) with clay-poor (red) and continuous clay-rich (blue) foresets with permeabilities of 1000 mD and 200 mD, respectively. B-D) Effective permeability (k_d , k_s , k_v) plotted against model sub-volume dimension: B) along depositional dip, C) along depositional strike, and D) vertically. Values of arithmetic and harmonic means, and the proportion of high-permeability lithology (clay-poor sandstone) are shown for comparison. Vertical and horizontal dashed lines show the REV dimension and the effective permeability, respectively, along the depositional dip, strike, and vertical directions.

and textural characteristics of the lithologies within the facies (Hossain et al., 2024). Clay-poor and clay-rich laminae occur in some cross-bedded and parallel-laminated sandstone facies (Sp, St, Spmc, Sh, Sl, Stl; Fig. 4A, B, C, D, H, K). These clay-poor and clay-rich laminae were directly sketched from outcrop photos, allowing us to assign distinct permeability values to each lamina type. This approach ensures a strong correlation between the measured permeability values and their spatial distribution within the model. Clay-poor and clay-rich sandstone laminae are assigned permeability values of 1000 mD and 200 mD, respectively, in planar and trough cross-bedded sandstone facies (Sp, St) (Fig. 4A, B). The same permeability values were used for clay-poor and clay-rich sandstone laminae in models of planar cross-bedded sandstone with mud clasts along foresets (Spmc), but mud clasts are treated as impermeable (Fig. 4C). In models of low-angle cross-bedded sandstone (Sl) and trough cross-laminated sandstone (Stl), clay-poor sandstone laminae are assigned permeability values of 800 mD and 160 mD, respectively, and clay-rich sandstone laminae are assigned permeability values of 200 mD and 40 mD (Fig. 4H, K). Clay-poor and clay-rich laminae in models of parallel-laminated sandstone (Sh) are assigned permeability values of 600 mD and 200 mD (Fig. 4D). Alternating strata of sandstone and mudstone or siltstone occur in other facies (Smd, Sss, Sc; Fig. 4E, G, L). In the mottled and deformed sandstone (Smd) and crinkly laminated sandstone (Sc) facies, sandstones are assigned permeability values of 400 mD and 200 mD, respectively, and mudstones are assigned a permeability value of 0.6 mD (Fig. 4E, L). In the fine-grained sandstone and siltstone facies (Sss), clay-rich and clay-poor sandstones have permeabilities of 20 mD and 60 mD, respectively. Pebbles in the matrix-supported conglomerate (Gmg) facies have 0.001 mD permeability whereas the sandstones have 50 mD permeability.

For the planar and trough cross-bedded sandstone facies (Sp, St), models of two cross-bedding scenarios were constructed. In one

scenario, clay-rich sandstone laminae were modelled as continuous foresets (Sp1, St1), while in the other scenario, they occur only over the lower half of the foresets (Sp2, St2). Dimensional data for facies-scale reservoir models were derived from cores, outcrops, and analogues reported in the published literature.

4.2. Model resolution

The required resolution for modeling different facies varies according to their geometrical complexity (Table 2). Mottled and deformed sandstone (Smd) facies, characterized by a complex network of sandstone lenses and sandstone-filled desiccation cracks, requires the highest model resolution. Similarly, trough cross-bedded sandstone (St), trough cross-laminated sandstone (Stl), planar cross-bedded sandstone with mudclasts along foresets (Spmc), and matrix-supported conglomerate (Gmg) facies also need high resolution due to their complex internal structures. Even layered facies such as parallel-laminated sandstone (Sh) and fine-grained sandstone and siltstone (Sss) facies require high resolution to capture thin layers. Crinkly laminated sandstone (Sc) facies require the lowest resolution.

4.3. REV definition and effective permeability

Figs. 5–7 present summaries of the reservoir models, REV dimensions and values of k_d , k_s , and k_v for trough cross-bedded sandstone with continuous clay-rich foresets (St1), parallel-laminated sandstone (Sh) and mottled and deformed sandstone (Smd) facies. Similar analysis and relevant plots for rest of the studied facies are attached as Supplementary Data. The facies-specific effective permeabilities and REV dimensions are compared in Figs. 8–10.

For the trough cross-bedded sandstone with continuous clay-rich

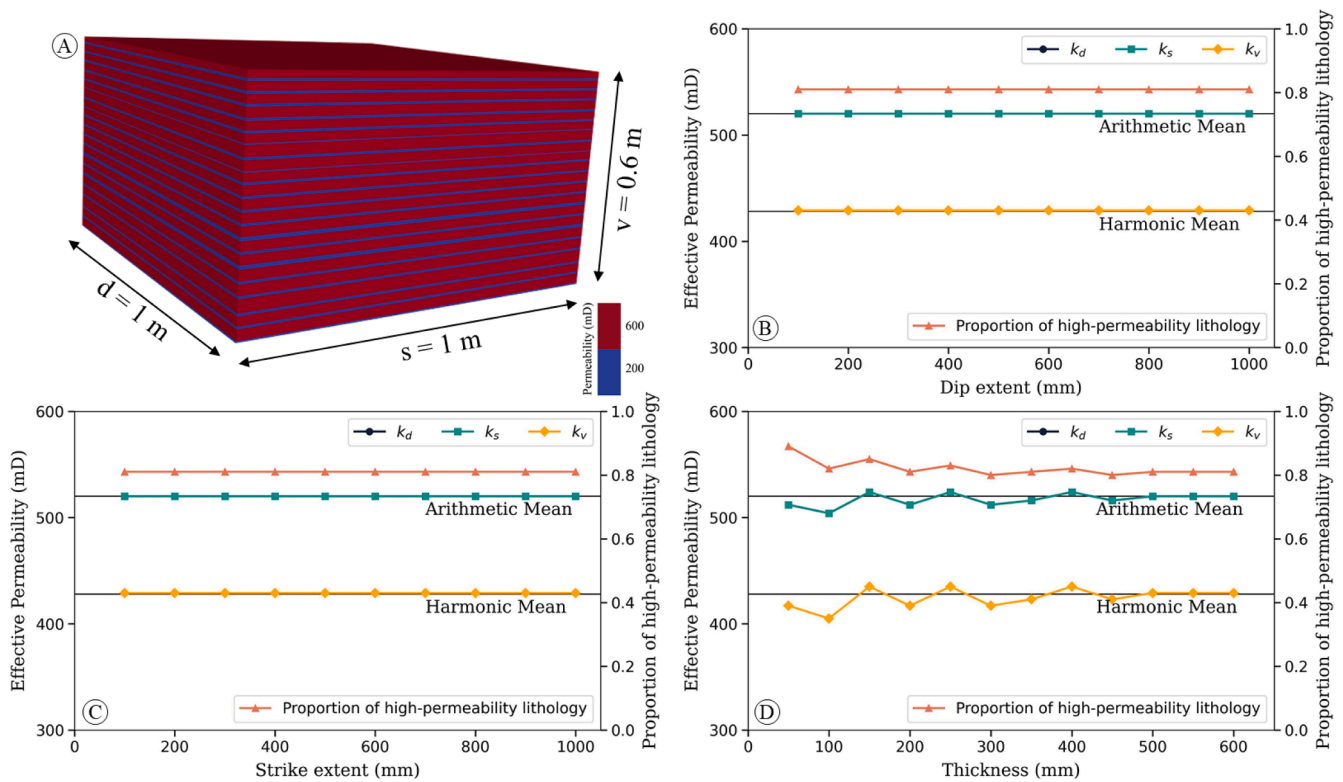


Fig. 6. A) Perspective view of the 3D model of the parallel-laminated sandstone facies (Sh; Table 1, Fig. 4D) with continuous clay-poor (red) and clay-rich (blue) laminae with permeabilities of 600 mD and 200 mD, respectively. B-D) Effective permeability (k_d , k_s , k_v) plotted against model sub-volume dimension: B) along depositional dip, C) along depositional strike, and D) vertically. Values of arithmetic and harmonic means, and the proportion of high-permeability lithology (clay-poor sandstone) are shown for comparison.

foresets (St1), REV dimensions are 1.5 m along depositional dip, 2.0 m along depositional strike, and 1.2 m vertically (Figs. 5 and 8). Effective permeability values are $k_d = 562$ mD, $k_s = 435$ mD, and $k_v = 452$ mD (Fig. 10). The k_d , k_s , and k_v values are all intermediate between the arithmetic and harmonic means (Fig. 5).

The parallel-laminated sandstone (Sh) facies is layered, and hence has no REV (Figs. 6 and 10). Effective permeability values are $k_d = 530$ mD, $k_s = 530$ mD, and $k_v = 400$ mD (Fig. 10). The k_d and k_s values are the same as the arithmetic mean, whereas the k_v value is equal to the harmonic mean (Fig. 6). The proportion of high-permeability lithology remains stable across different model sub-volume dimensions. These results are consistent with theory for layered systems (Renard and De Marsily, 1997; Dagan, 2012).

For the mottled and deformed sandstone (Smd), REV dimensions are 0.85 m along depositional dip, 0.4 m along depositional strike, and 0.35 m vertically (Figs. 7 and 8). Effective permeability values are $k_d = 141$ mD, $k_s = 153$ mD, and $k_v = 91$ mD (Fig. 10). Values of k_d , k_s , and k_v are intermediate between the arithmetic and harmonic means (Fig. 7). The proportion of high-permeability layers in model sub-volumes increases with increasing length along depositional dip and increasing thickness, and remains relatively stable with increasing width along depositional strike. Therefore, smaller models have lower effective permeability when cropped along depositional dip and vertically.

4.4. Impact of heterogeneity on REV dimensions

The REV dimensions of different facies vary in their depositional dip, depositional strike, and vertical dimensions, depending on the internal geometrical complexity of each facies (Figs. 5–7, S1–S9). A single permeability contrast, between low-permeability and high-permeability lithologies, was applied for each facies to determine the corresponding REV (Figs. 8 and 9). However, for facies Sp1 and St1, a range of

permeability contrasts was explored to assess their impact on REV dimensions. The findings indicate that varying the permeability contrast from a factor of 4 to 10 had minimal influence on the resulting REV dimensions. Even at high permeability contrasts above a factor of 40, there was no significant change observed in the REV dimensions. The REV dimensions and volumes reported above for each facies are summarised in Figs. 8 and 9. Trough cross-bedded sandstone facies (St1, St2) exhibits the largest REV (4.5 m^3), although planar cross-bedded sandstone (Sp1, Sp2) and low-angle cross-bedded sandstone facies (S1) have REV dimensions of comparable volume (Fig. 9). Smaller REV dimensions characterise crinkly laminated sandstone (Sc), mottled and deformed sandstone (Smd), trough cross-laminated sandstone (St1) and matrix-supported conglomerate (Gmg) facies, with volumes ranging between 0.01 and 0.1 m^3 . Even these small volumes are two orders of magnitude larger than the volume of a typical core plug ($3 \times 10^{-5}\text{ m}^3$; Fig. 9). Parallel-laminated sandstone (Sh) and fine-grained sandstone and siltstone (Sss) facies are layered and hence they do not have an REV, whereas laminated mudstone (Fl) and structureless sandstone (Sm) facies are homogenous.

Of two scenarios for both planar and trough crossbedded sandstone, those with discontinuous clay-rich foresets (Sp2, St2) have larger REV dimensions than those with continuous clay-rich foresets (Sp1, St1). Scenarios with continuous clay-rich sandstone foresets resemble layered systems such as parallel laminated sandstone (Sh) facies, resulting in a smaller REV compared to those in which the facies geometry differs from simple layering (cf. Jackson et al., 2003). Significant anisotropy is also observed between different scenarios. In planar cross-bedded sandstone (Sp), the REV in the depositional dip direction is seven times smaller in Sp1 than in Sp2 due to the pseudo-layered nature of the former.

From our results, it is evident that core plugs do not capture the REV for most facies in the Bunter Sandstone Formation (cf. Jackson et al., 2003, 2005; Massart et al., 2016). Core plug permeabilities will be adequate for characterisation of facies which are simply layered, or

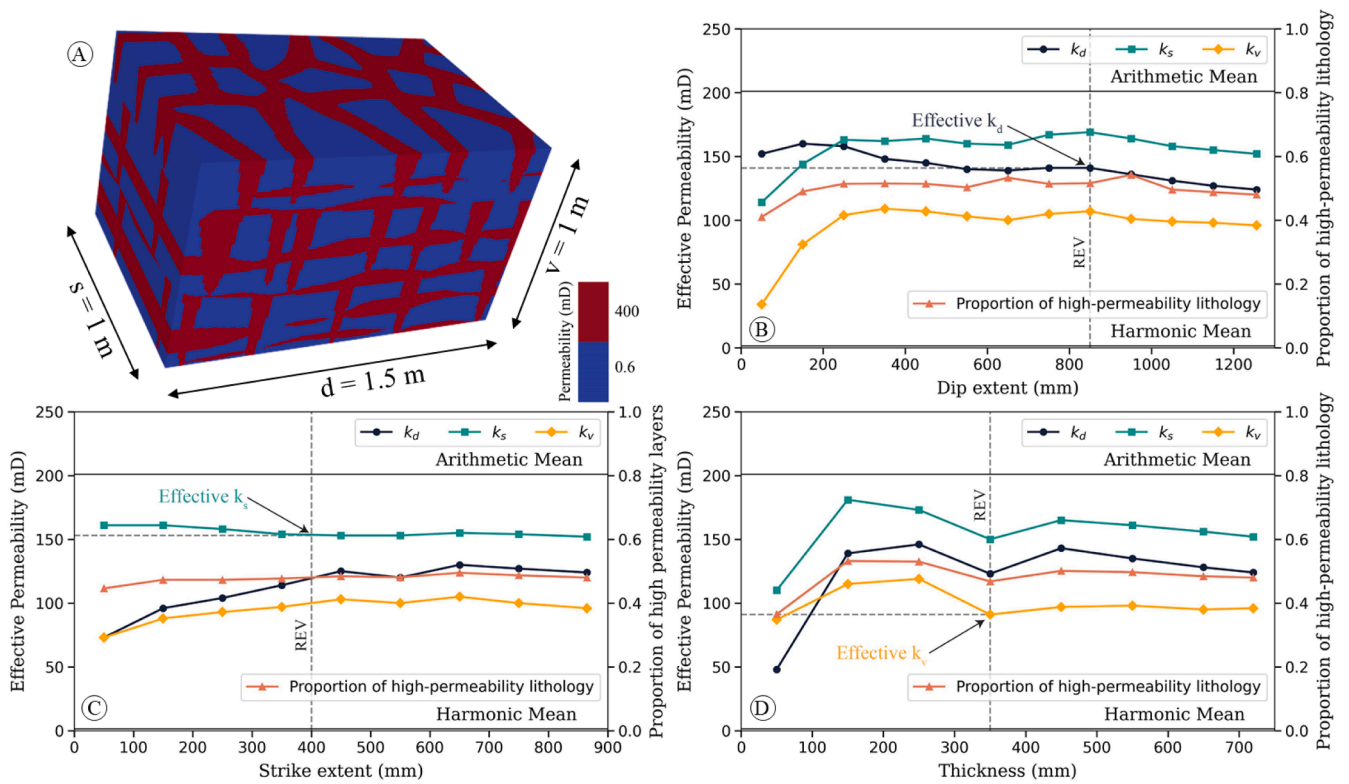


Fig. 7. A) Perspective view of the 3D model of the mottled and deformed sandstone facies (Smd; Table 1, Fig. 4E) with discontinuous, lenticular sandstones and sand-filled cracks (red) and mudstones (blue) with permeabilities of 400 mD and 0.6 mD, respectively. B-D) Effective permeability (k_d , k_s , k_v) plotted against model sub-volume dimension: B) along depositional dip, C) along depositional strike, and D) vertically. Values of arithmetic and harmonic means, and the proportion of high-permeability lithology (sandstone) are shown for comparison. Vertical and horizontal dashed lines show the REV dimension and the effective permeability, respectively, along the depositional dip, strike, and vertical directions.

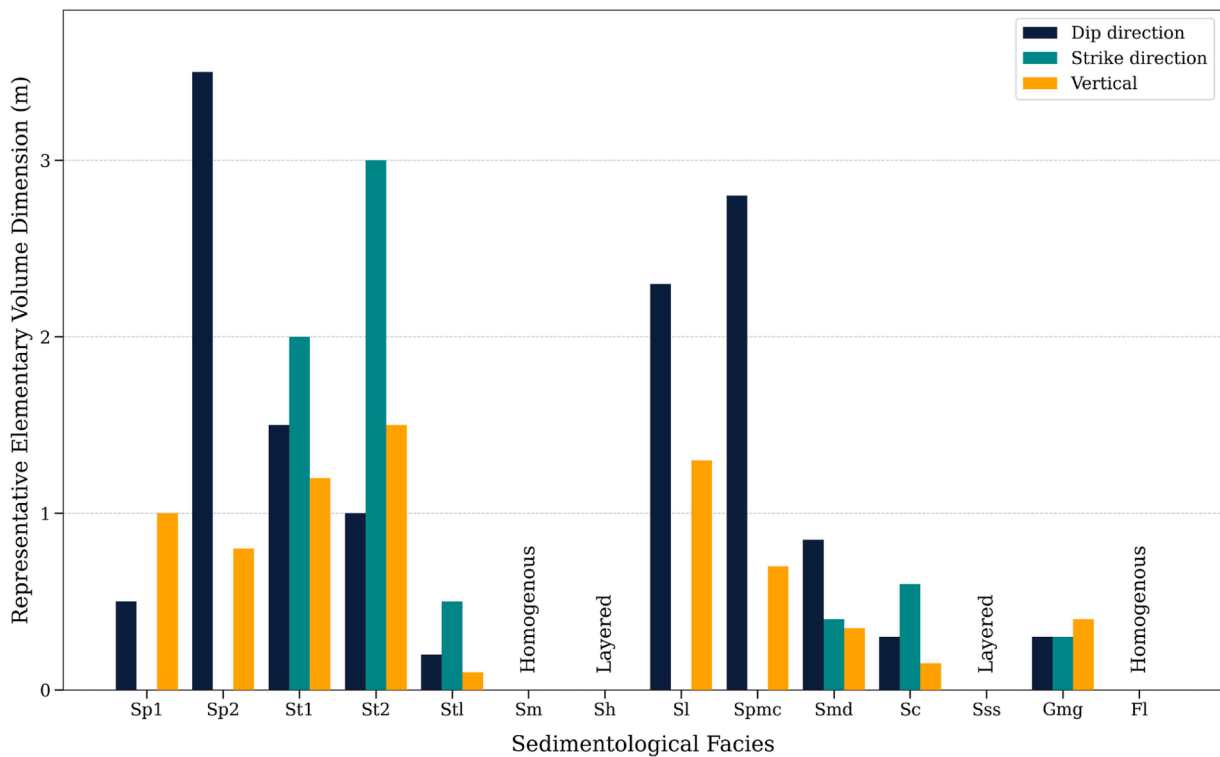


Fig. 8. REV dimensions of different facies (Table 1, Figs. 4–7, S1-S9) along depositional dip, depositional strike, and vertical directions.

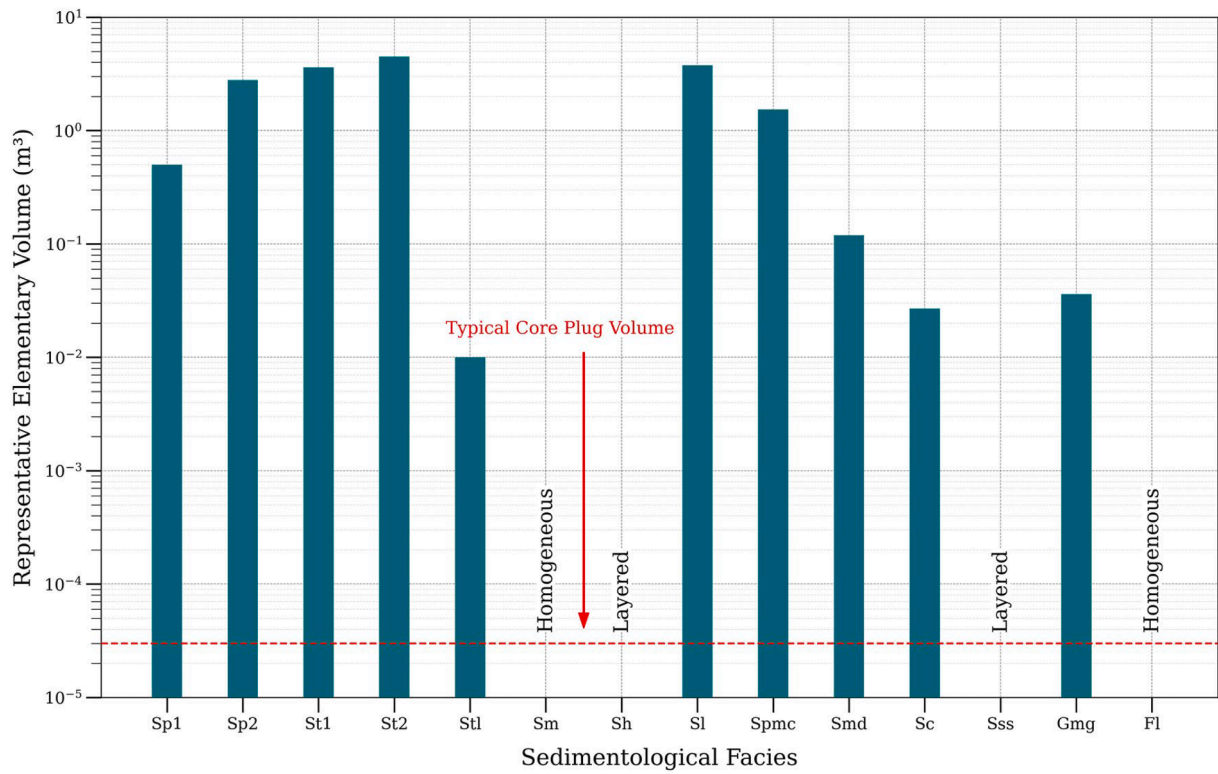


Fig. 9. REV volumes of different facies (Table 1, Figs. 4–7, S1-S9). The red line shows the volume of a typical core plug.

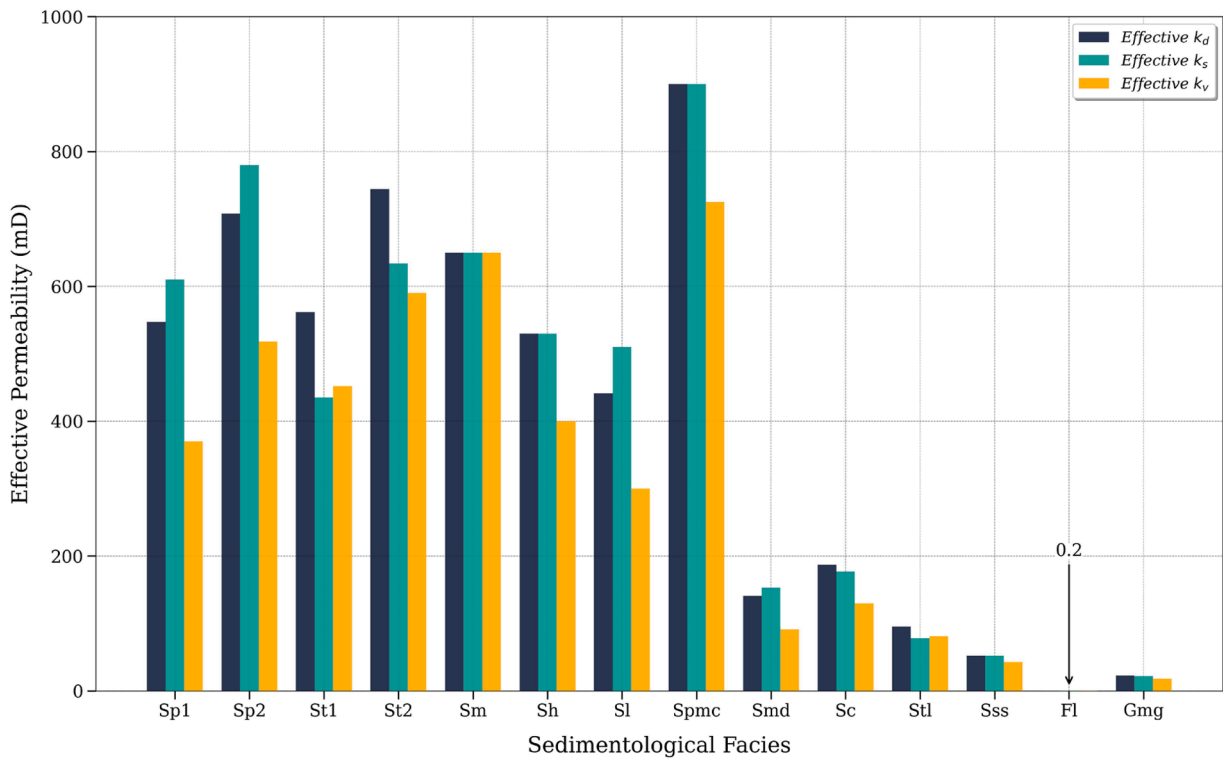


Fig. 10. Effective permeability of different facies (Table 1, Figs. 4–7, S1-S9) along depositional dip, depositional strike, and vertical directions (k_d , k_s and k_v , respectively).

uniform, isotropic systems, such as parallel-laminated sandstone (Sh), structureless sandstone (Sm), fine-grained sandstone and siltstone (Sss), and laminated mudstone (Fl) facies. However, significantly larger

volumes are required for cross-stratified facies (Sp, St, Sl, Spmc) (Fig. 9). Cross-bedded sandstone facies (St1, St2, Sp1, Sp2, Sl, Spmc) have effective permeabilities of 440–900 mD, 435–900 mD and 300–725 mD

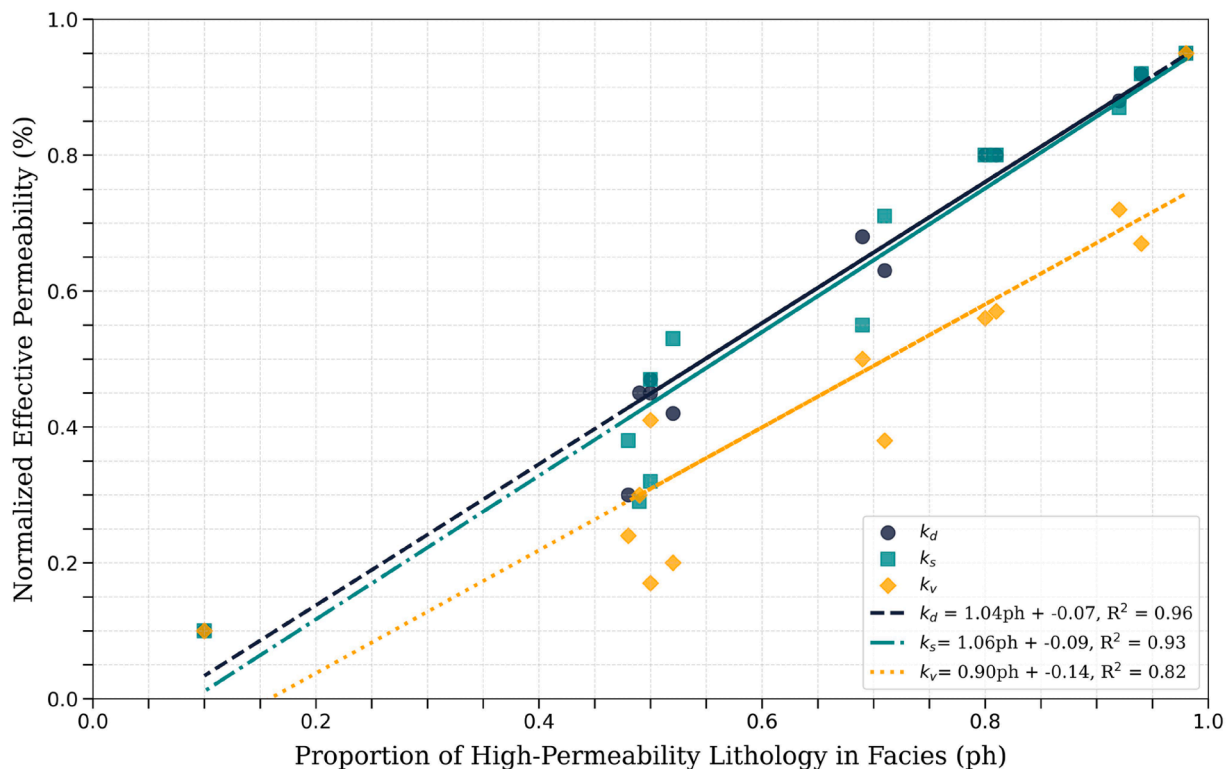


Fig. 11. Plot of normalized effective permeability at the largest model volume against the proportion of the high-permeability lithology in different facies (Table 1, Figs. 4–7, S1–S9).

in depositional dip, depositional strike and vertical directions (k_d , k_s and k_v), respectively (Fig. 10). Differences in effective permeability values between these facies reflect differences in the 3D geometry of cross-stratification and the occurrence and distribution of clay-rich sandstone laminae. Structureless sandstone (Sm) facies has an effective permeability of 650 mD in all directions. Planar laminated sandstone (Sh) facies has $k_d = k_s$ and k_v values of 530 mD and 400 mD (Fig. 10). Mottled and deformed sandstone (Smd), crinkly laminated sandstone (Sc), and fine-grained sandstone and siltstone (Sss) facies, which all contain siltstones, have significantly lower effective permeability values ($k_d = 52$ –187 mD, $k_s = 52$ –177 mD, $k_v = 43$ –130 mD). Laminated mudstone (Fl) and matrix-supported conglomerate (Gmg) have the lowest values of effective permeability, 0.2 mD and 17–23 mD, respectively (Fig. 10).

5. Discussion

5.1. Applications in subsurface modeling

5.1.1. Predicting permeability from core and wireline data

Core plug samples alone are insufficient to provide representative measurements of effective permeability for most facies. This limitation also applies to arithmetic, harmonic, and geometric mean values of permeability, which do not take geological heterogeneity and anisotropy into consideration. To obtain representative values, a substantial portion of the rock volume must be modeled using outcrop-informed geometries and architectures, a process that requires significant time and effort.

However, the proportion of high-permeability lithology in each facies exhibits a positive linear correlation with the normalized effective permeability (Eq. (1)) of the facies (Fig. 11). This relationship appears to be robust for k_d , k_s , and k_v , for proportions of high-permeability lithology of 0.4 to 1.0 (Fig. 11). Previous research established similar predictive relationships for effective permeability as a function of mudstone

content in heterolithic, wavy-bedded tidal sandstones using small-scale models (Jackson et al., 2003; Ringrose et al., 2005), but not in heterolithic cross-bedded tidal sandstones that contain mud drapes of variable and complex geometry, continuity and geometrical configuration (Massart et al., 2016). The effective permeability values and their correlation with the proportion of high-permeability lithology are accurate for the selected permeability values and contrasts observed in each facies. A variation of 10–15 % in effective permeability has been observed in facies Sp1 and St1 when the permeability contrast between the low-permeability and high-permeability lithologies are varied between factors of 2 and 10. However, when the permeability contrast exceeds a factor of 40, effective permeability can vary significantly for facies Sp1, depending on their geometrical characteristics. At higher permeability contrasts, changes in vertical effective permeability are more pronounced than those in horizontal effective permeability.

For the facies of the Bunter Sandstone Formation and Sherwood Sandstone Group, the relationship between the proportion of high-permeability lithologies, such as clay-poor sandstone (Sp, St, Spmc, Sh, Sl, Stl facies) or sandstone (Smd, Sss, Sc facies), and normalized effective permeability can be a powerful tool for reservoir characterization, potentially reducing the need for detailed facies modelling. Effective permeability can be estimated based simply on the proportion of high-permeability lithologies. While core data allow precise identification of the proportion of high-permeability lithologies, wireline logs, particularly image logs, can also be used to estimate their proportion, making it feasible to apply this method in subsurface analysis without extensive coring. However, more heterolithic facies (e.g., with larger extremes in permeability and more complex geometrical configurations) may not exhibit this simple relationship (Massart et al., 2016).

5.1.2. Predicting horizontal to vertical permeability ratio

The ratio of vertical to horizontal permeability (k_v/k_h) across different facies ranges from 0.38 to 1.0, for the selected permeability values and permeability contrasts (Fig. 12A). Horizontal permeability

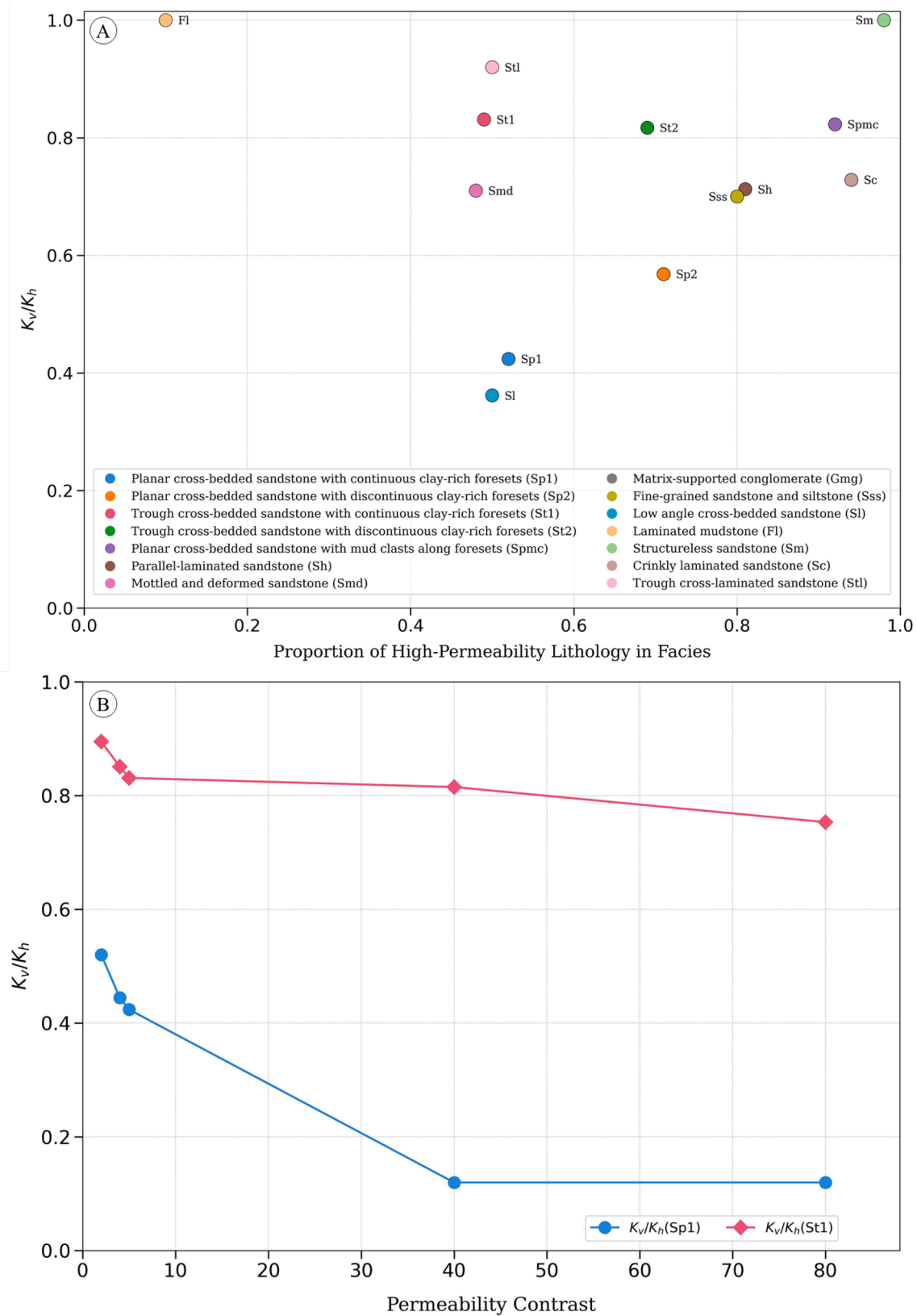


Fig. 12. A) Plot of k_v/k_h at the largest model volume against the proportion of the high-permeability lithology in different facies (Table 1, Figs. 4–7, S1 –S9). B) For Sp1 and St1, k_v/k_h ratio at multiple permeability contrasts are plotted.

(k_h) was calculated from the arithmetic mean of the k_d and k_s . Laminated mudstone (Fl) and structureless sandstone (Sm) facies show high k_v/k_h ratios, of 1.0, indicating isotropic permeability. In contrast, planar cross-bedded sandstone with continuous clay-rich foresets (Sp1) facies has lower k_v/k_h ratio, around 0.4. Intermediate k_v/k_h ratios are observed in trough cross-laminated sandstone (Stl) and planar cross-bedded sandstone with mud clasts (Spmc) facies, with values of approximately 0.7 and 0.5, respectively. In Sp1 and St1 facies, the k_v/k_h ratio shows minor variation when the permeability contrast between low-permeability and high-permeability lithologies is varied by factors of 4 to 10. However, at higher permeability contrasts, the facies architecture has a stronger influence on the k_v/k_h ratio. For instance, at a permeability contrast of 40, the k_v/k_h ratio in Sp1 decreases by 72 % compared to the ratio observed at a contrast of 5. In contrast, the reduction in k_v/k_h for St1 is only 7 % when the permeability contrast increases from 5 to 40 (Fig. 12B).

6. Conclusions

This study assessed the impact of sedimentological heterogeneity on the Representative Elementary Volume (REV) and calculated the effective permeability of twelve fluvial facies in the Bunter Sandstone Formation. Although there is significant variability in REV dimensions for different facies, larger rock volumes than standard core plugs are necessary for representative measurements in most facies, because they contain geometrically complex distributions of low- and high-permeability lithologies. Exceptions are layered (Sh, Ss) and homogeneous (Sm, Fl) facies for which the effective permeability can be calculated using simple weighted averaging. The largest REV is exhibited by trough cross-bedded sandstones (St1, St2), with dimensions ranging from 1.0 to 1.5 m, 2.0 to 3.0 m, and 1.2 to 1.5 m along depositional dip, depositional strike, and vertically, respectively. REV dimensions for planar cross-bedded sandstones (Sp1, Sp2) range from 0.5 to 3.5 m along depositional dip and 0.8 to 1.0 m vertically, while other cross-bedded facies (Sl, Spmc) have REV dimensions of 2.3 to 2.8 m along depositional dip and 1.3 to 0.7 m vertically.

Permeability anisotropy is observed, with distinct directional trends identified within most facies. The k_v/k_h ratio varies between 0.38 and 1.0 across different facies, with higher permeability contrasts significantly reducing k_v/k_h ratio in certain facies. For permeability measurements in low- and high-permeability lithologies measured in core using a minipermeameter, planar cross-bedded sandstone with mud clasts (Spmc) exhibits the highest effective horizontal (k_d , k_s) and vertical (k_v) permeabilities. Planar cross-bedded sandstones (Sp1, Sp2) and trough cross-bedded sandstones (St1, St2) also show high permeabilities. In contrast, facies such as crinkly laminated sandstone (Sc), fine-grained sandstone and siltstone (Sss), and mottled sandstone (Smd) exhibit moderate permeability, while laminated mudstones (Fl) and matrix-supported conglomerates (Gmg) are characterized by significantly lower effective permeability. A linear correlation is identified between the proportion of high-permeability lithologies (e.g., clay-poor sandstone) and normalized effective permeability (relative to the permeability of low- and high-permeability lithologies). Determining effective permeability is often challenging due to the need for detailed data and time-intensive workflows. In contrast, estimating the proportion of high-permeability lithologies is straightforward and quick. Therefore, the proportion of high-permeability lithologies, as determined from core data, can be used as a reliable predictor of effective permeability in the Bunter Sandstone Formation as well as in comparable Triassic fluvial deposits across northwestern Europe and other regions.

CRedit authorship contribution statement

Shakhawat Hossain: Writing – original draft, Visualization, Validation, Methodology, Investigation, Funding acquisition, Formal analysis, Conceptualization, Writing – review & editing. **Gary J. Hampson:** Writing – review & editing, Supervision, Methodology, Funding

acquisition, Conceptualization. **Carl Jacquemyn:** Writing – review & editing, Supervision, Software, Methodology, Conceptualization. **Matthew D. Jackson:** Writing – review & editing, Supervision, Methodology, Funding acquisition, Conceptualization. **Dmytro Petrovskyy:** Writing – review & editing, Software, Methodology. **Sebastian Geiger:** Writing – review & editing, Supervision, Methodology. **Julio D. Machado Silva:** Writing – review & editing, Software. **Sicilia Judice:** Writing – review & editing, Software. **Fazilatur Rahman:** Writing – review & editing, Software. **M. Costa Sousa:** Writing – review & editing, Software.

Declaration of competing interest

The authors declare that they have no known competing financial interests or personal relationships that could have appeared to influence the work reported in this paper.

Data availability

The Rapid Reservoir Modelling prototype (executable and source code) used to construct most of the facies-scale reservoir models is available at: <https://bitbucket.org/rapidreservoirmodelling/rm>. The 12 models used in this study are available at: https://figshare.com/articles/dataset/Models_effective_permeability_zip/27908148?file=50811252.

Acknowledgements

We are grateful for the constructive reviews of two anonymous reviewers, and the editorial handling of Francisco Valdés-Parada. This research was supported by a Bangabandhu Overseas Scholarship awarded to SH by the University of Dhaka, Bangladesh. We gratefully acknowledge the sponsors of the Rapid Reservoir Modelling (phase 2) consortium (ExxonMobil Upstream Research Company, Equinor, Petrobras, Petronas, and Shell), Energi Simulation for partial funding of a Chair for SG, and the British Geological Survey for providing access to core material from the Endurance reservoir. We also extend our thanks to Schlumberger Limited for the use of Petrel software via an academic software donation, as well as to the reviewers and editors for their valuable feedback.

Supplementary materials

Supplementary material associated with this article can be found, in the online version, at [doi:10.1016/j.advwatres.2025.104936](https://doi.org/10.1016/j.advwatres.2025.104936).

References

- Adams, B., Barker, J.A., Kitching, R., Miles, D.L., 1980. Thermal energy storage in permeable formations in the United Kingdom. *British Geological Survey, Report WD/ST/80/002*. <https://nora.nerc.ac.uk/id/eprint/517064>.
- Allen, D.J., Brewerton, L.J., Coleby, L.M., Gibbs, B.R., Lewis, M.A., MacDonald, A.M., Wagstaff, S.J., Williams, A.T., 1997. The physical properties of major aquifers in England and Wales. *British Geological Survey, Report WD/97/034*. <https://nora.nerc.ac.uk/id/eprint/13137>.
- Alshakri, J., Hampson, G.J., Jacquemyn, C., Jackson, M.D., Petrovskyy, D., Geiger, S., Silva, J.D.M., Judice, S., Rahman, F., Costa Sousa, M., 2023. A screening assessment of the impact of sedimentological heterogeneity on CO₂ migration and stratigraphic baffling potential: sherwood and Bunter sandstones, UK. In: Miodic, J.M., Heinemann, N., Edlmann, K., Alcalde, J., Schultz, R.A. (Eds.), *Enabling Secure Subsurface Storage in Future Energy systems*. Geological Society of London, Special Publication 528, pp. 245–266. <https://doi.org/10.1144/SP528-2022-34>.
- Ambrose, K., Hough, E., Smith, N.J.P., Warrington, G., 2014. Lithostratigraphy of the sherwood sandstone group of England, Wales and south-west Scotland. *British Geological Survey, Report RR/14/001*. <https://nora.nerc.ac.uk/id/eprint/507530>.
- Bear, J., 1972. *Dynamics of fluids in porous media*. American Elsevier, New York, pp. 756–p.
- Bertier, P., Swennen, R., Kemps, R., Laenen, B., Dreesen, R., 2022. Reservoir characteristics and diagenesis of the Buntsandstein sandstones in the Campine Basin (NE Belgium). *Geol. Belg.* 25, 145–184.

- Bloomfield, J.P., Moreau, M.F., Newell, A.J., 2006. Characterization of permeability distributions in six lithofacies from the Helsby and Wilmslow sandstone formations of the Cheshire Basin, UK. Barker, R.D. & Tellam, J.H. (Eds.), *Fluid Flow and Solute Movement in sandstones: the Onshore UK Permo-Triassic red Bed sequence*. Geological Society of London, Special Publication, 263, pp. 83–101.
- Bofill, L., Bozetti, G., Schäfer, G., Ghienne, J.-F., Schuster, M., Scherer, C., de Souza, E., 2024. Quantitative facies analysis of a fluvio-aeolian system: lower Triassic Buntsandstein Group, eastern France. *Sediment. Geol.* 465, 106634.
- Bossennec, C., Gérard, Y., Böcker, J., Klug, B., Mattioni, L., Bertrand, L., Moretti, I., 2021. Characterisation of fluid flow conditions and paths in the Buntsandstein Gp. sandstones reservoirs, Upper Rhine Graben. *Bulletin de la Société Géologique de France* 192, 35.
- Brookfield, M.E., 2004. The enigma of fine-grained alluvial basin fills: the Permo-Triassic (Cumbrian Coastal and Sherwood Sandstone Groups) of the Solway Basin, NW England and SW Scotland. *Int. J. Earth Sci.* 93, 282–296.
- Cecchetti, E., Martinus, A.W., Donselaar, M.E., Felder, M., & Abels, H.A. (2024). Sedimentology, stratigraphy and reservoir architecture of the lower triassic Main Buntsandstein in the Roer Valley Graben, The Netherlands. SSRN 4744988 [preprint].
- Cooke-Yarborough, P., 1991. The hewett field, blocks 48/28-29-30, 52/4a-5a, UK North Sea. Abbotts, L.L. In: *United Kingdom oil and Gas fields: 25 Years Commemorative Volume*, 14. Geological Society of London, Memoir, pp. 433–441.
- Corbett, P.W., Jensen, J.L., 1992. Variation of reservoir statistics according to sample spacing and measurement type for some intervals in the Lower Brent Group. *Log Anal.* 33. SPWLA-1992-v33n1a3.
- Costa Sousa, M., Silva, J.D.M., Silva, C.C.M.M., De Carvalho, F.M., Judice, S., Rahman, F., Jacquemyn, C., Pataki, M.E.H., Hampson, G.J., Jackson, M.D., Petrovskyy, D., Geiger, S., 2020. Smart modelling of geologic stratigraphy concepts using sketches. In: *Smart Tools and Applications in computer Graphics (STAG) 2020 Proceedings*, pp. 89–100. <https://doi.org/10.2312/stag.20201243>.
- Cowan, G., 1993. Identification and significance of aeolian deposits within the dominantly fluvial Sherwood Sandstone Group of the East Irish Sea Basin UK. In: North, C.P., Prosser, D.J. (Eds.), *Characterization of Fluvial and Aeolian reservoirs*. Geological Society, London, Special Publication 73, pp. 231–245.
- Dagan, G., 2012. *Flow and Transport in Porous Formations*. Springer Science & Business Media.
- Downing, R., Allen, D., Barker, J., Burgess, W., Gray, D., Price, M., Smith, I., 1984. Geothermal exploration at Southampton in the UK: a case study of a low enthalpy resource. *Energy Explor.* 2, 327–342.
- English, K.L., English, J.M., Moscardini, R., Houghton, P.D., Raine, R.J., Cooper, M., 2024. Review of triassic sherwood sandstone group reservoirs of Ireland and Great Britain and their future role in geoenery applications. *Geoenergy 2 geoenergy* 2023-2042.
- Gérard, A., Genter, A., Kohl, T., Lutz, P., Rose, P., Rummel, F., 2006. The deep EGS (Enhanced Geothermal System) project at Soultz-sous-Forêts, (Alsace, France). *Geothermics* 35, 473–483.
- Gluyas, J.G., Bagudu, U., 2020. The Endurance CO2 storage site, blocks 42/25 and 43/21, UK North Sea. Goffey, G. & Gluyas, J.G. In: *United Kingdom oil and Gas fields: 50th Anniversary Commemorative Volume*, 52. Geological Society of London, Memoir, pp. 163–171.
- Hartemink, E. (2021). *A Multi-Scale Reservoir Characterization of the Main Buntsandstein Subgroup in the Tilburg Area for Geothermal Operations*. Unpublished MS thesis, Civil Engineering & Geosciences, Delft University of Technology, <https://resolver.tudelft.nl/uuid:b3bb0590-e268-4a5b-ba78-a756fd71c547>.
- Heinemann, N., Wilkinson, M., Pickup, G.E., Haszeldine, R.S., Cutler, N.A., 2012. CO2 storage in the offshore UK Bunter Sandstone Formation. *Int. J. Greenhouse Gas Control* 6, 210–219.
- Helle, H.B., Bhatt, A., Ursin, B., 2001. Porosity and permeability prediction from wireline logs using artificial neural networks: a North Sea case study. *Geophys. Prospect.* 49, 431–444.
- Holliday, D., Jones, N., McMillan, A., 2008. Lithostratigraphical subdivision of the sherwood sandstone group (Triassic) of the northeastern part of the Carlisle Basin, Cumbria and Dumfries and Galloway, UK. *Scott. J. Geol.* 44, 97–110.
- Hollinsworth, A., de Jonge-Anderson, I., Underhill, J.R., Jamieson, R., 2024. Impact of reservoir quality on the carbon storage potential of the bunter sandstone formation, southern North Sea. *Geoenergy 2 geoenergy* 2023-2037.
- Holmslykke, H.D., Kjeller, C., Fabricius, I.L., 2021. Injection of Ca-depleted formation water in the lower triassic bunter sandstone formation for seasonal heat storage in geothermal sandstone reservoirs: effects on reservoir quality. *Geothermics* 96, 102179.
- Hossain, S., Hampson, G.J., Jacquemyn, C., Jackson, M.D., Chiarella, D., 2024. Permeability characterisation of sedimentological facies in the Bunter Sandstone Formation, Endurance CO2 storage site, offshore UK. *Int. J. Greenhouse Gas Control* 135, 104140.
- Hossain, S., Shekhar, H., Rahman, N., 2023. Facies and architectural element analysis of the upper bokabil sandstone in the Bengal Basin. *Sediment. Geol.* 453, 106433.
- Hounslow, M., Ruffell, A., 2006. Triassic: seasonal rivers, dusty deserts and saline lakes. In: Brenchley, P.J., Rawson, P.F. (Eds.), *The Geology of England and Wales*. Geological Society of London, pp. 295–324.
- Jackson, M.D., Muggeridge, A.H., Yoshida, S., Johnson, H.D., 2003. Upscaling permeability measurements within complex heterolithic tidal sandstones. *Math. Geol.* 35, 499–520.
- Jackson, M.D., Regnier, G., Staffell, I., 2024. Aquifer Thermal Energy Storage for low carbon heating and cooling in the United Kingdom: current status and future prospects. *Appl. Energy* 376, 124096.
- Jackson, M.D., Yoshida, S., Muggeridge, A.H., Johnson, H.D., 2005. Three-dimensional reservoir characterization and flow simulation of heterolithic tidal sandstones. *Am. Assoc. Pet. Geol. Bull.* 89, 507–528.
- Jacquemyn, C., Pataki, M.E.H., Hampson, G.J., Jackson, M.D., Petrovskyy, D., Geiger, S., Silva, J.D.M., Judice, S., Rahman, F., Silva, C.C.M.M., Costa Sousa, M., 2021. Sketch-based interface and modelling of stratigraphy and structure in three dimensions. *J. Geol. Soc. London* 178. <https://doi.org/10.1144/jgs2020-187>
- Kingdon, A., Fellgett, M., Spence, M., 2019. UKGEOs cheshire energy research field site: science infrastructure: version 2. In: *British Geological Survey, Report OR/19/052*. <https://nora.nerc.ac.uk/id/eprint/525100>.
- Lie, K.A., Møyner, O., & Krogstad, S. (2015). Application of flow diagnostics and multiscale methods for reservoir management. *Society of Petroleum Engineers, Paper 173376*. <https://doi.org/SPE-173306-MS>.
- Lottman, T. (2019). Determination of REV and effective properties of fluvial depositional systems: a feasibility study using 3D FLUMY models [unpublished MSc thesis].
- Mania, F.M. (2017). Estimation of permeability in siliciclastic reservoirs from well log analysis and core plug data; based on the data from an exploration well offshore Norway [unpublished MSc thesis].
- Martens, S., Liebscher, A., Möller, F., Hennings, J., Kempka, T., Lüthi, S., Norden, B., Prevedel, B., Szzybalski, A., Zimmer, M., Kühn, M., 2013. CO2 storage at the Ketzin pilot site, Germany: fourth year of injection, monitoring, modelling and verification. *Energy Procedia* 37, 6434–6443.
- Massart, B.Y., Jackson, M.D., Hampson, G.J., Johnson, H.D., 2016. Effective Flow Properties of heterolithic, Cross-Bedded Tidal sandstones: Part 2. Flow simulation, 100. American Association of Petroleum Geologists Bulletin, pp. 723–742.
- McKie, T., Williams, B., 2009. Triassic palaeogeography and fluvial dispersal across the northwest European Basins. *Geol. J.* 44, 711–741.
- Meadows, N., Beach, A., 1993. Controls on reservoir quality in the triassic sherwood sandstone of the Irish Sea. In: Parker, J.T. (Ed.), *Petroleum Geology of Northwest Europe: Proceedings of the 4th Conference*. Geological Society of London, *Petroleum Geology Conference Series* 4, pp. 823–833.
- Meckel, T.A., Bryant, S.L., Ganesh, P.R., 2015. Characterization and prediction of CO2 saturation resulting from modeling buoyant fluid migration in 2D heterogeneous geologic fabrics. *Int. J. Greenhouse Gas Control* 34, 85–96.
- Medici, G., Boulesteix, K., Mountney, N.P., West, L.J., Odling, N., 2015. Palaeoenvironment of braided fluvial systems in different tectonic realms of the triassic sherwood sandstone group, UK. *Sediment. Geol.* 329, 188–210.
- Medici, G., West, L., 2022. Review of groundwater flow and contaminant transport modelling approaches for the sherwood sandstone aquifer, UK; insights from analogous successions worldwide. *Q. J. Eng. Geol. Hydrogeol.* 55 qjehg2021-2176.
- Medici, G., West, L.J., Mountney, N.P., 2019. Sedimentary flow heterogeneities in the triassic UK Sherwood Sandstone Group: insights for hydrocarbon exploration. *Geol. J.* 54, 1361–1378.
- Møyner, O., Krogstad, S., Lie, K.-A., 2015. The application of flow diagnostics for reservoir management. *Soc. Pet. Eng. J.* 20, 306–323.
- Nordahl, K., Messina, C., Berland, H., Rustad, A.B., Rimstad, E., 2014. Impact of multiscale modelling on predicted porosity and permeability distributions in the fluvial deposits of the Upper Lunde Member (Snorre Field, Norwegian Continental Shelf). Martinus, A.W., Howell, J.A. & Good, T.R. In: *Sediment Body Geometry and Heterogeneity: Analogue Studies For Modelling the Subsurface*, 387. Geological Society of London, Special Publication, pp. 85–109.
- Nordahl, K., Ringrose, P.S., 2008. Identifying the representative elementary volume for permeability in heterolithic deposits using numerical rock models. *Math Geosci.* 40, 753–771.
- Noy, D., Holloway, S., Chadwick, R., Williams, J., Hannis, S., Lahann, R., 2012. Modelling large-scale carbon dioxide injection into the Bunter Sandstone in the UK Southern North Sea. *Int. J. Greenhouse Gas Control* 9, 220–233.
- Petrovskyy, D., Jacquemyn, C., Geiger, S., Jackson, M.D., Hampson, G.J., Silva, J.D.M., Judice, S., Rahman, F., Costa Sousa, M., 2023. Rapid flow diagnostics for prototyping of reservoir concepts and models for subsurface CO2 storage. *Int. J. Greenhouse Gas Control* 124, 103855.
- Pokar, M., West, L., Odling, N., 2006. Petrophysical characterization of the Sherwood sandstone from East Yorkshire, UK. Barker, R.D. & Tellam, J.H. *Fluid Flow and Solute Movement in sandstones: the Onshore UK Permo-Triassic red Bed sequence*. Geological Society of London 263, 103–118.
- Rasmussen, A., Lie, K., 2014. Discretization of flow diagnostics on stratigraphic and unstructured grids. In: *14th European Conference on the Mathematics of Oil Recovery*, 2014, pp. 1–17. <https://doi.org/10.3997/2214-4609.20141844>.
- Renard, P., De Marsily, G., 1997. Calculating equivalent permeability: a review. *Adv. Water Resour.* 20, 253–278.
- Ringrose, P., Nordahl, K., Wen, R., 2005. Vertical permeability estimation in heterolithic tidal deltaic sandstones. *Pet. Geosci.* 11, 29–36.
- Sansom, P.J., 1992. *Sedimentology of the Navajo Sandstone, Southern Utah, USA*. University of Oxford [unpublished PhD thesis].
- Shahvali, M., Mallison, B., Wei, K., Gross, H., 2012. An alternative to streamlines for flow diagnostics on structured and unstructured grids. *SPE Journal* 17, 768–778.
- Sorbier, A., 2024. Offshore CCS: a North Sea perspective from the Aramis Project. In: *85th European Association of Geoscientists and Engineers Annual Conference & Exhibition* [extended abstract].
- Vandeweyer, V., van der Meer, B., Kramers, L., Neele, F., Maurand, N., Le Gallo, Y., Bossie-Codré, D., Schäfer, F., Evans, D., Kirk, K., Bernstone, C., Stiff, S., Hull, W.,

2009. CO2 storage in saline aquifers: in the Southern North Sea and Northern Germany. *Energy Procedia* 1, 3079–3086.
- Wakefield, O.J., Hough, E., Peatfield, A.W., 2015. Architectural analysis of a triassic fluvial system: the sherwood sandstone of the East Midlands Shelf, UK. *Sediment. Geol.* 327, 1–13.
- Yousaf, H., Amjad, M., Claes, H., Swennen, R., Weltje, G.J., 2023. Assessment of Reservoir Quality and Heterogeneity in Middle Buntsandstein Sandstones of Southern Netherlands For Deep Geothermal Exploration [extended abstract].